The Center for Extended Magnetohydrodynamic Modeling

(Global Stability of Magnetic Fusion Devices)

S. Jardin—lead PI

GA: D. Brennan

MIT: L. Sugiyama, J. Ramos

NYU: B. Hientzsch, H. Strauss

PPPL: J. Breslau, J. Chen, G. Fu, W. Park, R. Samtaney

SAIC: D. Schnack, A. Pankin

TechX: S. Kruger

U. Colorado: S. Parker , D. Barnes

U. Wisconsin: A. Bayliss, J. Callen, C. Hegna, C. Sovinec

U. Utah: A. Sanderson

Utah State: J.-Y. Ji, E. Held

a SciDAC activity…

Partners with:

TOPS

TSTT

APDEC

SWIM

Outline

- List of CEMM students and postdocs and their projects/thesis topics
- List of CEMM publications and invited conference presentations
- CEMM SciDAC Partners
- Description of the project meetings
- Closures progress and prospects
- Progress in numerical methods and numerical benchmarks
- Update on Major Physics Studies:
  - Sawtooth Simulations (CDX-U)
  - ELM Modeling (DIII-D)
  - Energetic Particle Modes (ITER)
  - Pellet Simulations
- Projecting to the future

CEMM Educational Component

POSTDOCTORIAL RESEARCHERS:
Adam Bayliss—(U. Wisc) Code development and algorithms for fluid-based closures, and applications.

Charlson Kim (U.Wisc/U.Washington) Implemented NIMROD's hot-particle kinetics.

Bernhard Hientzsch (NYU) Working on spectral elements (SEL) for M3D.

Jeong-Yong Ji (Utah State) Deriving neoclassical parallel closures primarily for NTMs

GRADUATE STUDENTS:
Hao Tian (U.Wisc) Development for Hall electric field: two-fluid tearing and dynamo.

Jim Reynolds (U. Wisc) Applying NIMROD to study transients in reversed-field pinch plasmas.

Chris Carey (U. Wisc) Applying NIMROD to study stability and relaxation of jet-like configurations.

Nick Murphy (U.Wisc) Applying NIMROD for modeling reconnection in MRX and SSX.

Nukta Sharma (Utah State) Deriving neoclassical parallel closures primarily for NTMs

Nate Ferraro (Princeton) The effect of the gyroviscocus force on equilibrium and stability

Slava Lukin (Princeton) Application of spectral element methods to the non-ideal internal kink.

Sterling Smith (Princeton) Development of realistic equilibrium for ELM simulations

Mamood Miah (Princeton) Numerical stability of implicit techniques using high-order finite elements

CEMM Publications (A-M) May 2005-May 2006

- Brennan DP, Kruger et al, “A categorization of tearing mode onset in tokamaks via nonlinear simulation”, Nucl. Fus. 45 1178 (Sep 2005)
- Chen, J, Jardin, SC, Strauss HR “Solving anisotropic transport equation on misaligned grids”, Computational Science-ICCS 2005, PT 3 3516 1076 (2005) in Lecture Notes in Computer Science
- Chen J, Strauss HR, Jardin S, et al, Application of Mass Lumped Higher Order Finite Element”, PPPL-4128
- Chen J, Strauss HR, Jardin SC, et al, “Higher Order Lagrange FiniteElements in M3D”, PPPL4032
- Cohen BI, .., Sovinec CR, et al, “Simulation of spheromak evolution and energy confinement”, Phys. Plasmas 12 056106 (May 2005)
- Ferraro N and Jardin S, “Finite element implementation of Braginskii’s gyroviscous stress with application to the gravitational instability (April 2006, submitted to Phys. Plasmas)
- Fu GY, Park W, Strauss H, et al, “Global Hybrid Simulations of Energetic Particle Effects on the n=1 Mode in Tokamaks: Internal Kink and Fishbone Instability” to appear in Phys Plasmas
- Fu G, Breslau J. Fredrickson E. et al, “Global Hybrid Simulations of Energetic Particle-driven Modes in Toroidal Plasmas, PPPL 4029
- Jardin SC and Breslau JA: “Implicit solution of the four-field extended MHD equations using high-order high-continuity finite elements”, Phys. Plasmas 12 056101 (May 2005)
- Hooper EB, …, Sovinec CR, et al, “Magnetic reconnection during flux conversion in a driven spheromak”, Phys. Plasmas 12 092503 (Sep 2005)
- Kruger SE, Schnack DD, Sovinec CR, “Dynamics of the major disruption of a DIII-D plasma”, Phys Plasmas 12 056113 (May 2005)
- Menard JE,Park W, et al “Internal kink mode dynamics in high-beta NSTX plasmas”, Nucl. Fus. 45 539 (Jul 2005)

CEMM Publications (N-Z) May 2005-May 2006

- Pankin A. Y. Bateman G., Brennan DP, et al., “Elm triggering conditions for the integrated modeling of H-mode plasmas”, Czech. J. of Physics 55 367 (Mar 2005)
- Ramos JJ, “General expression of the gyroviscous force”, Phys. Plasma 12 112301 (Nov 2005)
- Ramos JJ, “Fluid formalism for collisionless magnetized plasmas”, Phys Plasma. 12 052102 (May 2005)
- Ryutov DD, …, Sovinec CR, et al, “The effect of artificial diffusivity on the flute instability” Phys. Plasmas 12 084504 (Aug 2005)
- Samtaney R. , S. C. Jardin, P. Colella, and D. F. Martin, Adaptive Mesh Refinement Methods for Magnetic Fusion Applications. Published in Adaptive Mesh Refinement: Theory and Applications, Lecture Notes in Computational Science and Engineering. Editors: Plewa, Linde and Weirs. Springer-Verlag, 2005.
- Samtaney R., P. Colella, T. J. Ligocki, D. F. Martin and S. C. Jardin, An adaptive mesh semi-implicit conservative method for resistive MHD. Journal of Physics, Conference Series, SciDAC 2005, Vol 16, pp: 40-48, 2005.
- Sovinec CR, Schnack DD, Pankin AY et al., “Nonlinear Extended Magnetohydrodynamics Simulation Using High-Order Finite Elements,” Journal of Physics: Conference Series **16**, 25 (IoP, London, 2005).
- Reynolds D., R. Samtaney and C. S. Woodward, “A Fully Implicit Numerical Method for Single-Fluid Resistive Magnetohydrodynamics”, J. of Comput. Phys., to appear 2006.
- Schnack DD, Barnes DC, Brennan DP et al, “Computational Modeling of Fully Ionized Magnetized Plasmas using the Fluid Approach”, Phys. Plasmas 12 (to appear) 2006
- Turnbull AD, Brennan DP, Chu MS, et al. , “Theory and simulation basis for MHD stability in DIII-D”, Fus. Sci. and Tech 48 875 (Oct 2005)
- Wheatley V, Pullin DI, Samtaney R, “Stability of an impulsively accelerated density interface in magnetohydrodynamics”, Phys. Rev. Lett. 95 125002 (Sept 2005)
- Woodruff S, …,Sovinec CR, et al, “Controlled and spontaneous magnetic field generation in a gun-driven spheromak”, Phys. Plasmas 12 052502 (May 2005)

CEMM Major Invited Talks May 2005-May 2006

- S. Jardin, “Finite Element Calculations of the Magnetohydrodynamics of Magnetic Fusion Devices and Magnetic Reconnection”, (Invited Paper at the International Parallel Computational Fluid Dynamics Conference 2005, College Park, MD)
- R. Samtaney “An adaptive mesh semi-implicit conservative method for resistive MHD” SciDAC 2005, San Francisco
- C. R. Sovinec “Nonlinear Extended Magnetohydrodynamics Simulation Using High-Order Finite Elements,” SciDAC 2005 San Francisco.
- D. Schnack “Computational Modeling of Fully Ionized Magnetized Plasmas using the Fluid Approach”, (Invited Tutorial paper, 2005 APS/DPP meeting, Denver, CO)
- R. Samtaney, “Tokamak Pellet Fueling Simulations using 3D Adaptive Mesh Refinement”, (Invited paper, 2005 APS/DPP meeting, Denver, CO)
- S. Jardin, “Towards Comprehensive Simulation of Fusion Plasmas”, (Keynote applications talk at DOE conference on “Frontiers of Extreme Computing, Santa Cruz, CA)
- J.-Y Ji, “Parallel closures for transport applications”, (Invited Paper at APS/Sherwood 2006 April Meeting, Dallas, TX)

CEMM SciDAC Partners

(both current and 2006 letters of support)

PI	Center	Topic
P. Colella	APDEC	AMR- General Support of Chombo
D. Keyes	TOPS	Optimized Solvers, Implicit Techniques
L. Diachin	ITAPS/TSTT	Adaptive Methods, Optimized Meshes
R. Samulyak	SAPP/ITAPS	Pellet ablation via front tracking
K. Jansen (RPI)	SAPP/ITAPS	Adaptive Meshing for M3D-C^1 code
H. Yee (NASA)	SAPP/CEMM	Low Dissipative Methods for MHD
D. Schissel	Collaboratory	Collaboration Software
L. Sugiyama	Collaboratory	Collaboration and Data access
A. Kritz	Multi-Scale Integrated Plasma Simulations	Bringing MHD into Integrated Models
H. Strauss	SAPP/ITAPS	Optimal Mesh Generation
R. Samtaney	SAPP/APDEC	AMR-Pellet Injection / ELMs
D. Batchelor	SWIM	MHD into RF/MHD Integrated Model

CEMM Meetings May 05-May 06

- Oct 22-23 CEMM pre-APS meeting, (Denver CO)
  - 22 30 min presentations
  - session on test problems
  - Joint Sessions with SWIM and CPES
- Jan 25-26 Fluid Modeling of ELMs (Boulder, CO)
  - 18 presentations
  - participation by experimentalists, analytic theorists, and computational physicists
- Mar 22-24 Closures Workshop (ORNL)
  - Workshop was requested by DOE
  - 10 invited and 14 contributed talks
  - Good participation by analytic theorists
  - Good discussion of test problems
  - Excellent session on MHD Research Strategy for next 10 years
- April 25th CEMM post-Sherwood meeting, (Dallas, TX)
  - 12 20 min presentations
  - Supplement to Closures Workshop

Closure Progress and Prospects-1

- NIMROD and M3D-C^1 now have full (Braginskii) gyroviscous tensor and 2-fluid terms incorporated and are verifying these on test problems

Present since Day 1

Recently been added and tested

Still being developed (|| closures)

$$\frac{\partial n}{\partial t} + \nabla \bullet (n\vec{V}) = 0$$

$$\frac{\partial \vec{B}}{\partial t} = -\nabla \times \vec{E} \qquad \vec{J} = \nabla \times \vec{B}$$

$$nM_i\left(\frac{\partial \vec{V}}{\partial t} + \vec{V} \bullet \nabla \vec{V}\right) + \nabla p = \vec{J} \times \vec{B} - \nabla \bullet \Pi_{GV} - \nabla \bullet \Pi_{\parallel} - \nabla \bullet \Pi_{\perp}$$

$$\vec{E} + \vec{V} \times \vec{B} = \frac{1}{ne}\left(\vec{R} + \vec{J} \times \vec{B} - \nabla p_e - \nabla \bullet \vec{\vec{\Pi}}^{e}_{\parallel}\right)$$

$$\frac{3}{2}\frac{\partial p_e}{\partial t} + \nabla \bullet \left(\frac{3}{2} p_e \vec{V}\right) = -p_e \nabla \bullet \vec{V} + \frac{\vec{J}}{ne} \bullet \left[\frac{3}{2}\nabla p_e - \frac{5}{2}\frac{p_e}{n}\nabla n + \vec{R} - \nabla \bullet \vec{\vec{\Pi}}_e\right] - \nabla \bullet \vec{q}_e + Q_\Delta$$

$$\frac{3}{2}\frac{\partial p_i}{\partial t} + \nabla \bullet \left(\frac{3}{2} p_i \vec{V}\right) = -p_i \nabla \bullet \vec{V} - \Pi_i : \nabla V - \nabla \bullet \vec{q}_i - Q_\Delta$$

- Several approaches are being pursued to develop the parallel (||) closures in a computationally tractable form

Closure Progress and Prospects-2

Several approaches are being pursued to develop the parallel (||) closures in a computationally tractable form

- Braginskii (improved by Catto and Simakov) developed collisional regime closures: not valid in plasma core
- Hammett and Perkins, and later Beer, Snyder, et al have proposed Landau-type closures: formulated in terms of *k*-space
- Barnes and the M3D group have proposed PIC-type δf closures: but high order moments tend to be noisy
- E. Held, et al, are developing continuum techniques to calculate parallel heat flow and the parallel stress tensor from the solution of the parallel kinetic equation: work in progress, very compute intensive
- D. Spong is developing a neoclassical closure method based on using DELTA5D and/or DKES to compute viscosity coefficients for insertion into M3D
- Sugiyama has implemented a neoclassical closure based on the anisotropic temperature evolution equations of Snyder, et al
- Hegna and Gianakon have developed a heuristic neoclassical closure

Closure Progress and Prospects-3

There are two generic types of extended MHD problems (J. Callen, Closures Workshop 2006, SWIM proposal, 2005):

- Fast MHD ($\omega > \nu_I \sim 10^3\ s^{-1}$) phenomena occur on *Alfven* timescale
  - Sawtooth, Disruption, ELMs: Only need 2-fluid + GV

- Slow MHD ($\omega < \nu_I \sim 10^3\ s^{-1}$) phenomena occur on *dissipative* timescale
  - NTM, RWM: All transport effects important, need parallel closures

Our strategy is to pursue applications in the Fast MHD area as we work to better refine models and algorithms in the Slow MHD area.

In addition: Other approaches are being evaluated to incorporate sub-grid, presently unresolved physics

- Projective Integration (Kevrekidis, et al)
- Coupling MHD with drift wave turbulence (Diamond & McDevitt)

Progress in Numerical Methods and Numerical Benchmarks

- Code Development Overview
- 2-fluid algorithms in NIMROD and M3D-C^1
- Tests of the 2-fluid + gyroviscous model
  - 2-fluid tearing in slab geometry for range of Δ'
  - Gravitational Instability[1]
- Particle/Fluid Hybrid Benchmarks
  - Comparison of M3D and NIMROD models
- Nonlinear Benchmarks
  - GEM reconnection problem
  - CDX-U sawtooth [in applications section]

[1]Suggested by D. Schnack (Roberts and Taylor 1963)

Code Development Overview:

Code	Geom.	Development Emphasis
NIMROD	torus or slab	2-fluid, GV, non gyro-averaged particles, improved density evolution
M3D	torus	HO & spectral elements, new mesh generation, upwinding density, vector-friendly elliptic solver
M3D-C^1	slab	GV , V&V, adaptive mesh, 3D extension
AMRMHD[a] (Samtaney)	torus or slab	Implicit methods, vacuum region, improved pellet physics
SEC[b] (Glasser/Lukin)	slab	Rezoning to an optimal mesh

[a] In conjunction with APDEC

[b] Not funded by CEMM, but participates in test problems

NIMROD: Implementation of the implicit leapfrog is nearly complete.

- Hall and implicit advection terms are fully implemented.
- Linear parts of Braginskii gyroviscosity and heat drifts are complete; nonlinear terms are under development.
- Matrix-free solves of non-Hermitian 3D systems have been implemented; approximate 2D systems are formed and solved for preconditioning.

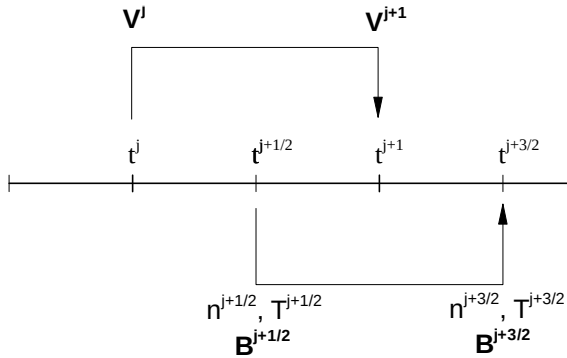

$$m_i n^{j+1/2}\left(\frac{\Delta \mathbf{V}}{\Delta t}+\frac{1}{2}\mathbf{V}^j\cdot\nabla\Delta\mathbf{V}+\frac{1}{2}\Delta\mathbf{V}\cdot\nabla\mathbf{V}^j\right)-\Delta t L^{j+1/2}(\Delta\mathbf{V})+\nabla\cdot\Pi_i(\Delta\mathbf{V})=\mathbf{J}^{j+1/2}\times\mathbf{B}^{j+1/2}$$
$$-m_i n^{j+1/2}\mathbf{V}^j\cdot\nabla\mathbf{V}^j-\nabla p^{j+1/2}-\nabla\cdot\Pi_i\left(\mathbf{V}^j\right)$$

$$\frac{\Delta n}{\Delta t}+\frac{1}{2}\nabla\cdot\left(\mathbf{V}^{j+1}\cdot\Delta n-D\nabla\Delta n\right)=-\nabla\cdot\left(\mathbf{V}^{j+1}\cdot n^{j+1/2}-D\nabla n^{j+1/2}\right)$$

$$\frac{3n}{2}\left(\frac{\Delta T_\alpha}{\Delta t}+\frac{1}{2}\mathbf{V}_\alpha^{j+1}\cdot\nabla\Delta T_\alpha\right)+\frac{n}{2}\Delta T_\alpha\nabla\cdot\mathbf{V}_\alpha^{j+1}+\frac{1}{2}\nabla\cdot\mathbf{q}_\alpha(\Delta T_\alpha)$$
$$=-\frac{3n}{2}\mathbf{V}_\alpha^{j+1}\cdot\nabla T_\alpha^{j+1/2}-nT_\alpha^{j+1/2}\nabla\cdot\mathbf{V}_\alpha^{j+1}-\nabla\cdot\mathbf{q}_\alpha\left(T_\alpha^{j+1/2}\right)+Q_\alpha^{j+1/2}$$

$$\frac{\Delta\mathbf{B}}{\Delta t}-\frac{1}{2}\nabla\times\left(\mathbf{V}^{j+1}\times\Delta\mathbf{B}\right)+\frac{1}{2}\nabla\times\frac{1}{ne}\left(\mathbf{J}^{j+1/2}\times\Delta\mathbf{B}+\Delta\mathbf{J}\times\mathbf{B}^{j+1/2}\right)+\frac{1}{2}\nabla\times\eta\Delta\mathbf{J}$$
$$=-\nabla\times\left[\frac{1}{ne}\left(\mathbf{J}^{j+1/2}\times\mathbf{B}^{j+1/2}-\nabla p_e\right)-\mathbf{V}^{j+1}\times\mathbf{B}^{j+1/2}+\eta\mathbf{J}^{j+1/2}\right]$$

- Tests show that we need to revisit the spatial representation of p_e, however.

M3D-C^1 code has very similar implicit time advance as NIMROD for full Extended MHD (2-fluid) equations-- time step determined by accuracy only:

$$\begin{bmatrix} S^v_{11} & S^v_{12} & S^v_{13} \\ S^v_{21} & S^v_{22} & S^v_{23} \\ S^v_{31} & S^v_{32} & S^v_{33} \end{bmatrix} \bullet \begin{bmatrix} U \\ V_z \\ \chi \end{bmatrix}^{n+1} = \begin{bmatrix} D^v_{11} & D^v_{12} & D^v_{13} \\ D^v_{21} & D^v_{22} & D^v_{23} \\ D^v_{31} & D^v_{32} & D^v_{33} \end{bmatrix} \bullet \begin{bmatrix} U \\ V_z \\ \chi \end{bmatrix}^{n} + \begin{bmatrix} R^v_{11} & R^v_{12} & R^v_{13} \\ R^v_{21} & R^v_{22} & R^v_{23} \\ R^v_{31} & R^v_{32} & R^v_{33} \end{bmatrix} \bullet \begin{bmatrix} \psi \\ I \\ T_e \end{bmatrix}^{n}$$

$$\vec{V} = \nabla U \times \hat{z} + \nabla_\perp \chi + V_z$$
$$\vec{B} = \nabla \psi \times \hat{z} + I\hat{z}$$

Alfven Wave physics

$$S^n_{11} \bullet N^{n+1} = D^n_{11} \bullet N^n + \begin{bmatrix} R^n_{11} & R^n_{12} & R^n_{13} \end{bmatrix} \bullet \begin{bmatrix} U \\ V_z \\ \mathrm{X} \end{bmatrix}^{n+1} + \begin{bmatrix} Q^n_{11} & Q^n_{12} & Q^n_{13} \end{bmatrix} \bullet \begin{bmatrix} U \\ V_z \\ \mathrm{X} \end{bmatrix}^{n} + Q^n_{14}$$

density

$$S^p_{11} \bullet P^{n+1} = D^p_{11} \bullet P^n + \begin{bmatrix} R^p_{11} & R^p_{12} & R^p_{13} \end{bmatrix} \bullet \begin{bmatrix} U \\ V_z \\ \mathrm{X} \end{bmatrix}^{n+1} + \begin{bmatrix} Q^p_{11} & Q^p_{12} & Q^p_{13} \end{bmatrix} \bullet \begin{bmatrix} U \\ V_z \\ \mathrm{X} \end{bmatrix}^{n} + Q^p_{14}$$

pressure

$$\begin{bmatrix} S^p_{11} & S^p_{12} & S^p_{13} \\ S^p_{21} & S^p_{22} & S^p_{23} \\ S^p_{31} & S^p_{32} & S^p_{33} \end{bmatrix} \bullet \begin{bmatrix} \psi \\ I \\ T_e \end{bmatrix}^{n+1} = \begin{bmatrix} D^p_{11} & D^p_{12} & D^p_{13} \\ D^p_{21} & D^p_{22} & D^p_{23} \\ D^p_{31} & D^p_{32} & D^p_{33} \end{bmatrix} \bullet \begin{bmatrix} \psi \\ I \\ T_e \end{bmatrix}^{n} + \begin{bmatrix} R^p_{11} & R^p_{12} & R^p_{13} \\ R^p_{21} & R^p_{22} & R^p_{23} \\ R^p_{31} & R^p_{32} & R^p_{33} \end{bmatrix} \bullet \begin{bmatrix} U \\ V_z \\ \chi \end{bmatrix}^{n+1} + \begin{bmatrix} Q^p_{11} & Q^p_{12} & Q^p_{13} \\ Q^p_{21} & Q^p_{22} & Q^p_{23} \\ Q^p_{31} & Q^p_{32} & Q^p_{33} \end{bmatrix} \bullet \begin{bmatrix} U \\ V_z \\ \chi \end{bmatrix}^{n}$$

Whistler, KAW, field diffusion physics

NIMROD: Two-fluid Reconnection: Linear Tearing in Slab Geometry

- V. Mirnov, C. Hegna, and S. Prager apply asymptotics to sheared slab configurations over a wide range of parameters. [Phys. Pl. **11**, 4481 (2004)]
- The study extended and connected previous research on linear two-fluid tearing with a large guide field (B_z component).
- Using the new implicit leapfrog, we have run NIMROD on computations in conditions of large and small Δ' and large and small β.

	input					*output*		
CASE	$\Delta' L$	$k L$	β	ρ_s / L	$S \equiv \tau_r / \tau_a$	δ / L	$\Gamma \equiv \gamma \tau_a / k\rho_s$	Γ_{ana}*
A	0.28	0.93	0.002	0.56	6.7×10^{3}	0.184	8.51×10^{-3}	$\Gamma_{(54)}= 9.04\times10^{-3}$ $\Gamma_{(55)}=1.30\times10^{-2}$
B	0.28	0.93	0.083	3.6	6.7×10^{3}	0.172	1.50×10^{-3}	$\Gamma_{(56)}=1.61\times10^{-3}$
C	5.3	0.33	0.083	3.6	670	0.11	0.106	$\Gamma_{(73)}=0.109$
D	5.3	0.33	0.083	3.6	67	0.25	0.203	$\Gamma_{(73)}=0.221$
E	5.3	0.33	0.083	3.6	6.7	0.65	0.297	$\Gamma_{(73)}=0.379$
F	24	0.083	0.083	3.6	6.7	1.11	0.401	$\Gamma_{(68)}=0.550$
G	5.3	0.33	0.83	11.4	6.7	0.48	0.169	$\Gamma_{(73)}= 0.0928$

Comparison of computed growth rates (Γ) with analytical relations (Γ_{ana}) show good agreement when the reconnection layer (δ) is smaller than the equilibrium scale (L).

Tests of the 2-fluid and Gyroviscous terms: Gravitational Instability

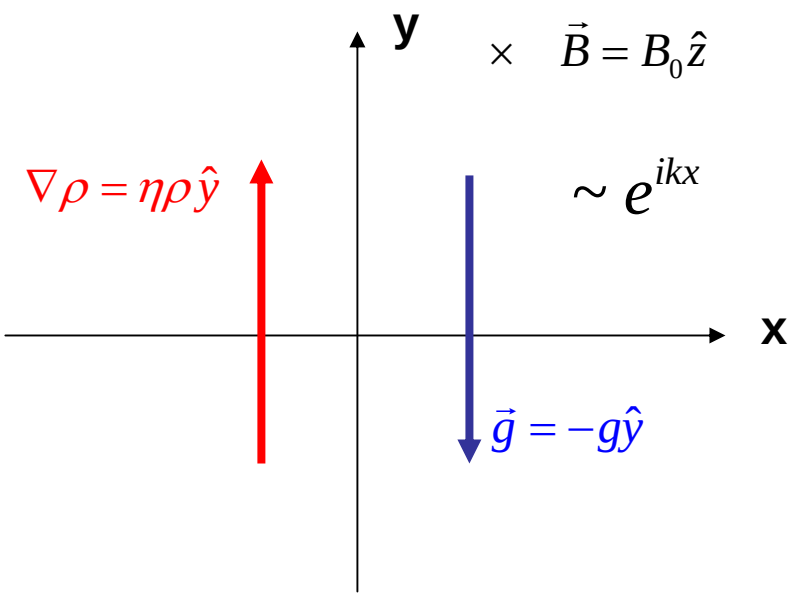

$$\frac{\partial\rho}{\partial t} + \nabla\bullet(\rho\vec{V}) = 0 \qquad p = p_i(\rho)$$

$$\frac{\partial\vec{B}}{\partial t} = \nabla\times\left[\vec{V}\times\vec{B} - \frac{1}{ne}\left(\vec{J}\times\vec{B}\right)\right] \qquad \vec{J} = \nabla\times\vec{B}$$

$$nM_i\left(\frac{\partial\vec{V}}{\partial t} + \vec{V}\bullet\nabla\vec{V}\right) + \nabla p = \vec{J}\times\vec{B} - \nabla\bullet\Pi_{GV}$$

Low-β result (R&T)

$$\omega^2 - \omega_*\omega + \gamma_{MHD}^2 = 0$$

$$\omega_* = \omega_{*2F} + \omega_{*GV}, \quad \gamma_{MHD}^2 = \frac{g}{L}$$

$$\omega_{*2F} = \frac{gk}{\Omega}, \quad \omega_{*GV} = \frac{1}{2}\frac{\rho_i^2k^2}{kL}\Omega$$

$$\omega = \frac{1}{2}\left(\omega_* \pm \sqrt{\omega_*^2 - 4\gamma_{MHD}^2}\right)$$

Stable if: $\omega_* > 2\gamma_{MHD}$

Braginskii gyro-viscosity in M3D-*C*[1]:

$$\nabla\cdot\vec{\vec{\Pi}} = \left\{\left[\nabla\times\left(\frac{mp}{eB^2}\vec{B}\right)\right]\cdot\nabla\right\}\vec{V} - \nabla\left[\frac{mp}{2eB^2}\vec{B}\cdot\left(\nabla\times\vec{V}\right)\right] - \nabla\times\left\{\frac{mp}{eB^2}\left[(B\cdot\nabla)\vec{V} + \frac{1}{2}\left(\nabla\cdot\vec{V} - \frac{3}{B^2}\vec{B}\cdot\left[\left(\vec{B}\cdot\nabla\right)\vec{V}\right]\right)\vec{B}\right]\right\}$$
$$+(B\cdot\nabla)\left\{\frac{mp}{eB^2}\left(\frac{3}{B^2}\vec{B}\times\left[\left(\vec{B}\cdot\nabla\right)\vec{V}\right] + \frac{3}{2B^2}\left[\vec{B}\cdot\left(\nabla\times\vec{V}\right)\right]\vec{B} - \nabla\times\vec{V}\right)\right\}$$

Ramos

$$\hat{z}\cdot \quad\rightarrow\quad [V_z,\alpha I] - \alpha\left\{\left[\psi,\nabla_\perp^2 U\right] + \left[\frac{\partial\psi}{\partial x},\frac{\partial U}{\partial x} - \frac{\partial\chi}{\partial y}\right] + \left[\frac{\partial\psi}{\partial y},\frac{\partial U}{\partial y} + \frac{\partial\chi}{\partial x}\right]\right\} - \frac{\partial\alpha}{\partial x}\left[\psi,\frac{\partial U}{\partial x} - \frac{\partial\chi}{\partial y}\right] - \frac{\partial\alpha}{\partial y}\left[\psi,\frac{\partial U}{\partial y} + \frac{\partial\chi}{\partial x}\right]$$
$$+\frac{1}{2}\alpha\nabla_\perp^2\chi\nabla_\perp^2\psi + \frac{1}{2}\left(\alpha\nabla_\perp^2\chi,\psi\right) - \frac{1}{2}\left[(\gamma\kappa,\psi) + \gamma\kappa\nabla_\perp^2\psi\right] + [\gamma\xi_z,\psi] + \frac{1}{2}[\lambda I,\psi] + \left[\alpha\nabla_\perp^2 U,\psi\right]$$

$$-\hat{z}\cdot\nabla\times \quad\rightarrow\quad \left[\frac{\partial\chi}{\partial x} + \frac{\partial U}{\partial y},\frac{\partial(\alpha I)}{\partial y}\right] - \left[\frac{\partial\chi}{\partial y} - \frac{\partial U}{\partial x},\frac{\partial(\alpha I)}{\partial x}\right] + \left[\nabla_\perp^2 U,\alpha I\right] + \nabla_\perp^2\left\{\alpha[\psi,V_z]\right\} - \frac{1}{2}\nabla_\perp^2\left(\alpha I\nabla_\perp^2\chi\right) + \frac{1}{2}\nabla_\perp^2(\gamma\kappa I)$$
$$+\frac{\partial}{\partial y}[\gamma\xi_x,\psi] - \frac{\partial}{\partial x}\left[\gamma\xi_y,\psi\right] + \frac{1}{2}\left\{\frac{\partial\lambda}{\partial x}\left[\frac{\partial\psi}{\partial x},\psi\right] + \frac{\partial\lambda}{\partial y}\left[\frac{\partial\psi}{\partial y},\psi\right] + \left([\lambda,\psi],\psi\right) + \left[\lambda\nabla_\perp^2\psi,\psi\right]\right\} + \frac{\partial}{\partial x}\left[\psi,\alpha\frac{\partial V_z}{\partial x}\right] + \frac{\partial}{\partial y}\left[\psi,\alpha\frac{\partial V_z}{\partial y}\right]$$

$$\nabla\cdot \quad\rightarrow\quad \left[\frac{\partial\chi}{\partial x} + \frac{\partial U}{\partial y},\frac{\partial(\alpha I)}{\partial y}\right] + \left[\frac{\partial\chi}{\partial y} - \frac{\partial U}{\partial x},\frac{\partial(\alpha I)}{\partial y}\right] + \left[\nabla_\perp^2\chi,\alpha I\right] + \frac{1}{2}\nabla_\perp^2\left\{\alpha\left[I\nabla_\perp^2 U - (\psi,V_z)\right]\right\} + \frac{\partial}{\partial x}[\gamma\xi_x,\psi] + \frac{\partial}{\partial y}\left[\gamma\xi_y,\psi\right]$$
$$+\frac{1}{2}\left[[\lambda,\psi],\psi\right] + \lambda\left[\frac{\partial\psi}{\partial y},\frac{\partial\psi}{\partial x}\right] + \frac{1}{2}\frac{\partial\lambda}{\partial x}\left[\frac{\partial\psi}{\partial y},\psi\right] - \frac{1}{2}\frac{\partial\lambda}{\partial y}\left[\frac{\partial\psi}{\partial x},\psi\right] + \frac{\partial}{\partial x}\left\{\alpha\left[\psi,\frac{\partial V_z}{\partial y}\right]\right\} - \frac{\partial}{\partial y}\left\{\alpha\left[\psi,\frac{\partial V_z}{\partial x}\right]\right\} + \left[V_z,[\alpha,\psi]\right]$$

$$\alpha \equiv \frac{ep}{mB^2} = \frac{ep/m}{\left(\frac{\partial\psi}{\partial x}\right)^2 + \left(\frac{\partial\psi}{\partial y}\right)^2 + I^2}$$

$$\gamma = \frac{3ep/m}{\left[\left(\frac{\partial\psi}{\partial x}\right)^2 + \left(\frac{\partial\psi}{\partial y}\right)^2 + I^2\right]^2}$$

$$\vec{\xi} = \left\{\frac{\partial\psi}{\partial x}[\psi,V_z] + I\left[\psi,\frac{\partial\chi}{\partial y} - \frac{\partial U}{\partial x}\right]\right\}\hat{x} + \left\{\frac{\partial\psi}{\partial y}[\psi,V_z] - I\left[\psi,\frac{\partial\chi}{\partial x} + \frac{\partial U}{\partial y}\right]\right\}\hat{y}$$

$$\lambda = \gamma\left[(\psi,V_z) - I\nabla_\perp^2 U\right]$$

$$\kappa \equiv \frac{\partial\psi}{\partial y}\left[\frac{\partial\chi}{\partial x} + \frac{\partial U}{\partial y},\psi\right] - \frac{\partial\psi}{\partial x}\left[\frac{\partial\chi}{\partial y} - \frac{\partial U}{\partial x},\psi\right] + I[V_z,\psi]$$

$$-\left\{\frac{\partial\psi}{\partial x}\left[\psi,\frac{\partial\chi}{\partial x} + \frac{\partial U}{\partial y}\right] + \frac{\partial\psi}{\partial y}\left[\psi,\frac{\partial\chi}{\partial y} - \frac{\partial U}{\partial x}\right]\right\}\hat{z}$$

Breslau

M3D-C^1 Gravitational Instability stabilized by Gyroviscosity

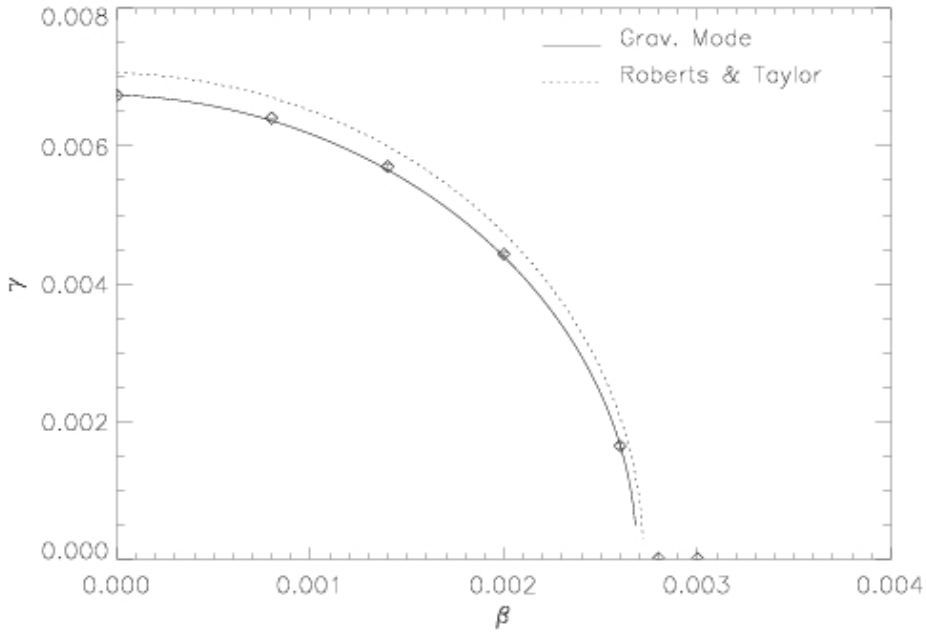

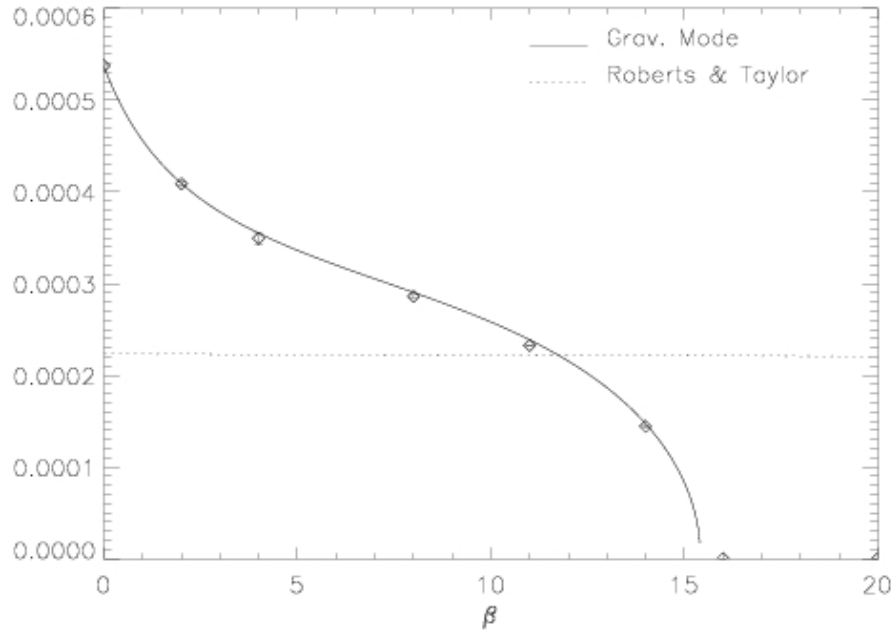

We have calculated the stabilization of the gravitational instability by Gyroviscosity: low beta (left) and high beta (right)

Ferraro

M3D-C^1…Gravitational Instability: nonlinear

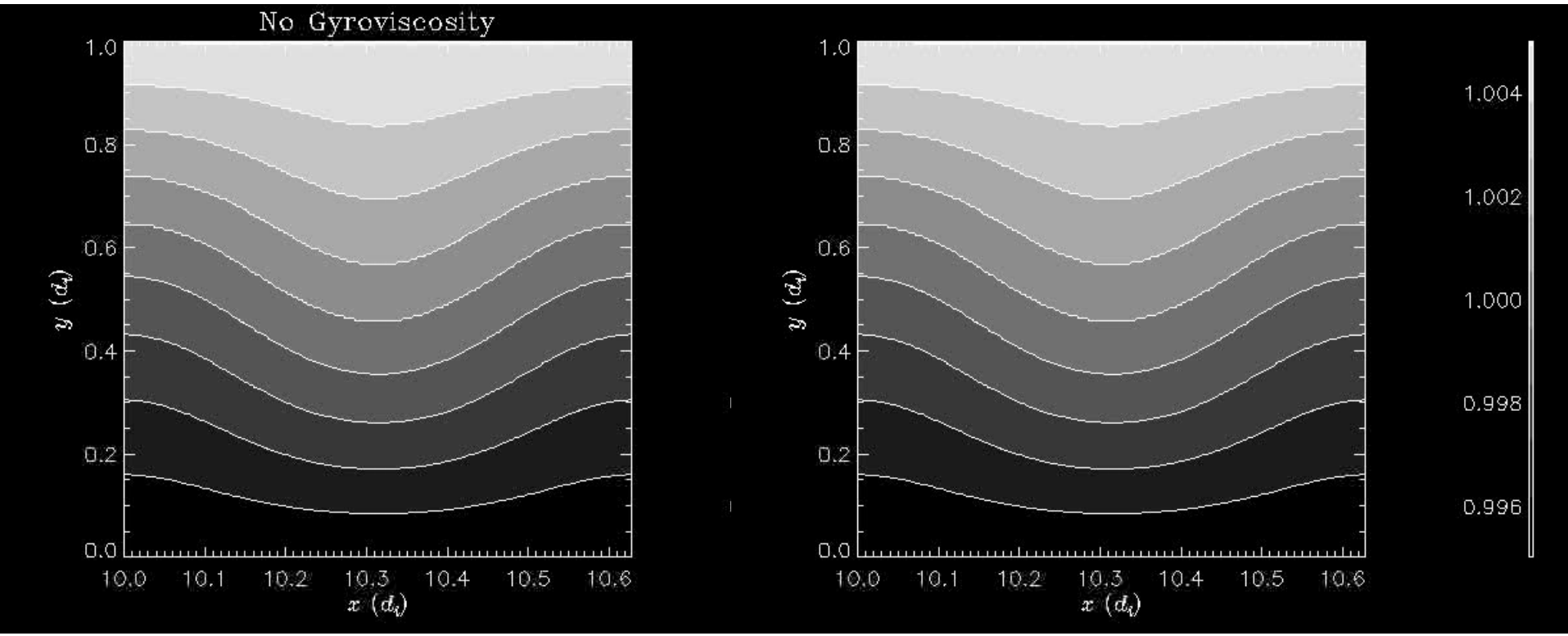

Ferraro

2-fluid *g*-mode in NIMROD

- Validation of NIMROD on *g*-mode problem
- 2-fluid only
- Fully compressible
- Walls placed far away
- Get good agreement with theory on both 2-fluid stability threshold and MHD growth rate
- Found heuristic time step CFL limit:
  $\omega_{*MAX}\Delta t < 1/4$
- Still working on GV validation

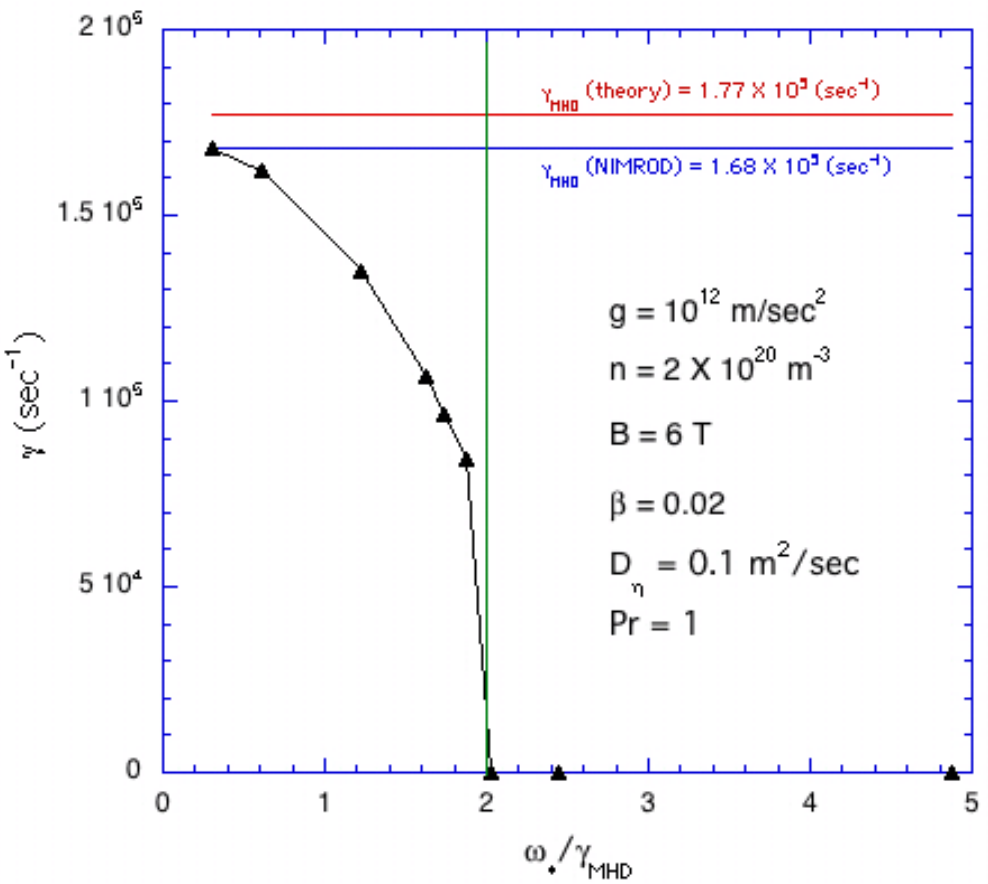

Schnack

Particle/Fluid Benchmarks

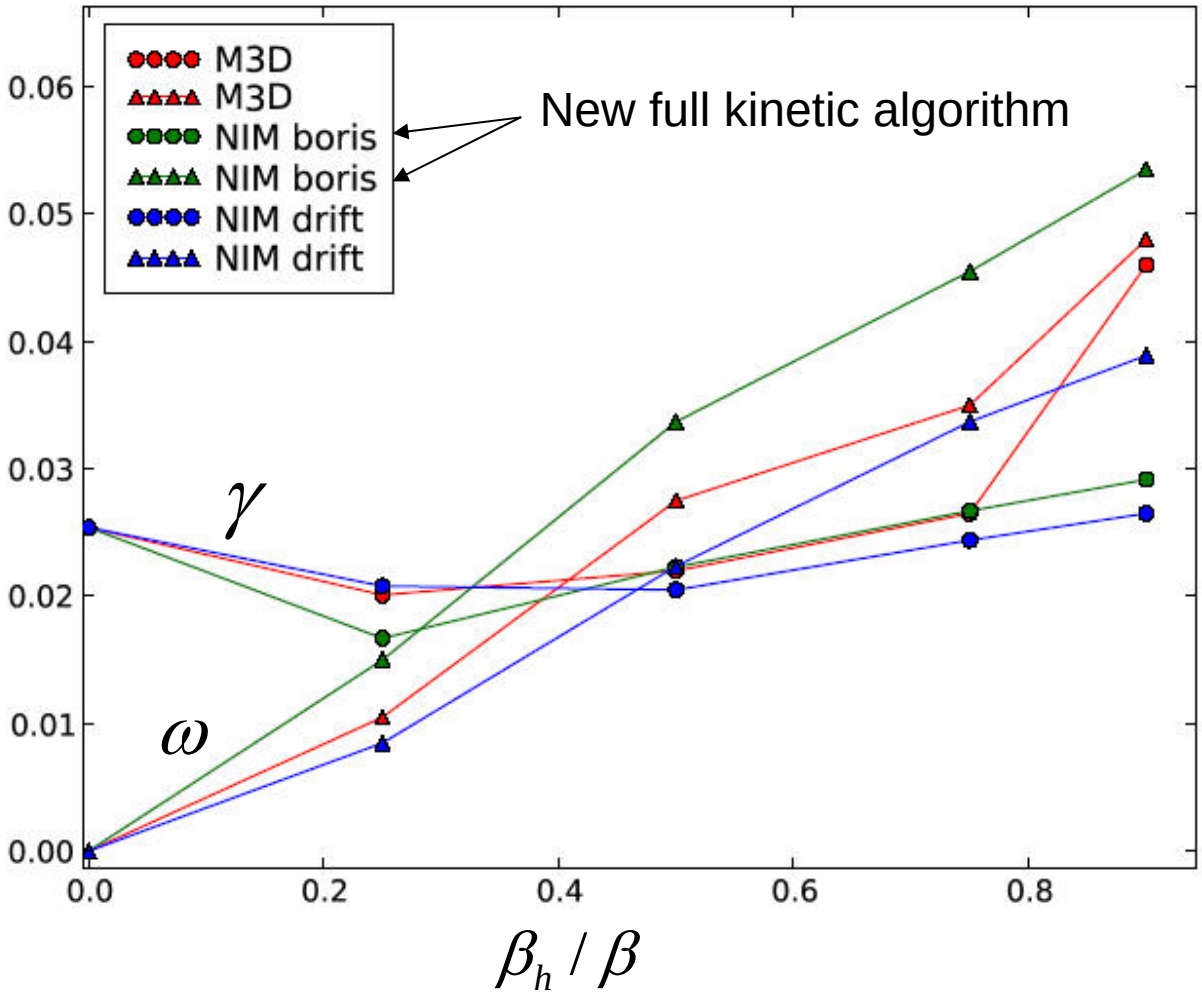

NIMROD has implemented a non-gyro-averaged particle push (Boris) for use in alternative concepts (FRC's, etc)

GEM Nonlinear Benchmark

Poloidal Flux Ψ

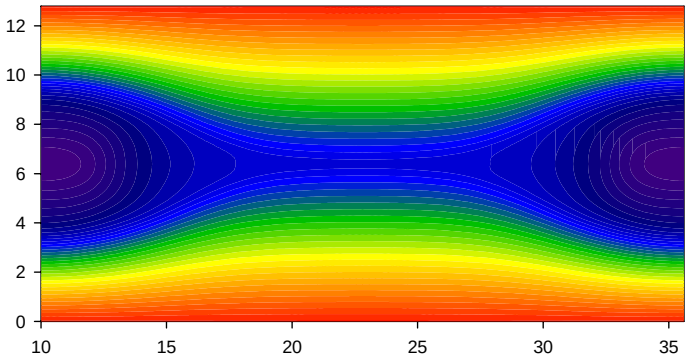

Current Density J

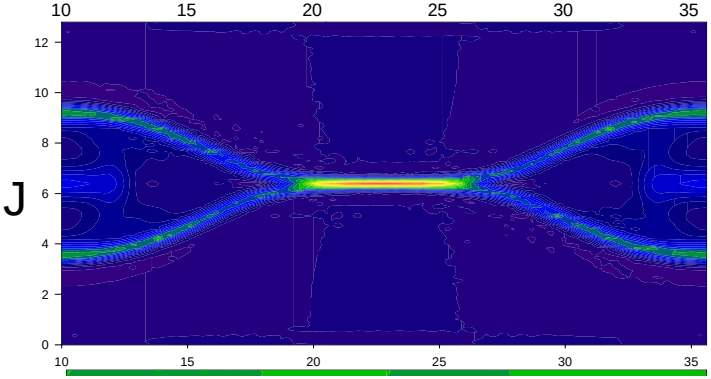

GEM Reconnection Problem

$$\psi^0(x,y) = \frac{1}{2}\ln(\cosh 2y),$$

$$\tilde{\psi}(x,y) = \varepsilon \cos k_x x \cos k_y y$$

1. High Viscosity μ = 10 η
2. Low Viscosity μ = 0.1 η
3. Two-Fluid (in progress)

We are comparing results from different codes in detail using the same (a) physics model, (b) geometry, and (c) boundary conditions as a means of code validation and verification

Nonlinear Benchmark

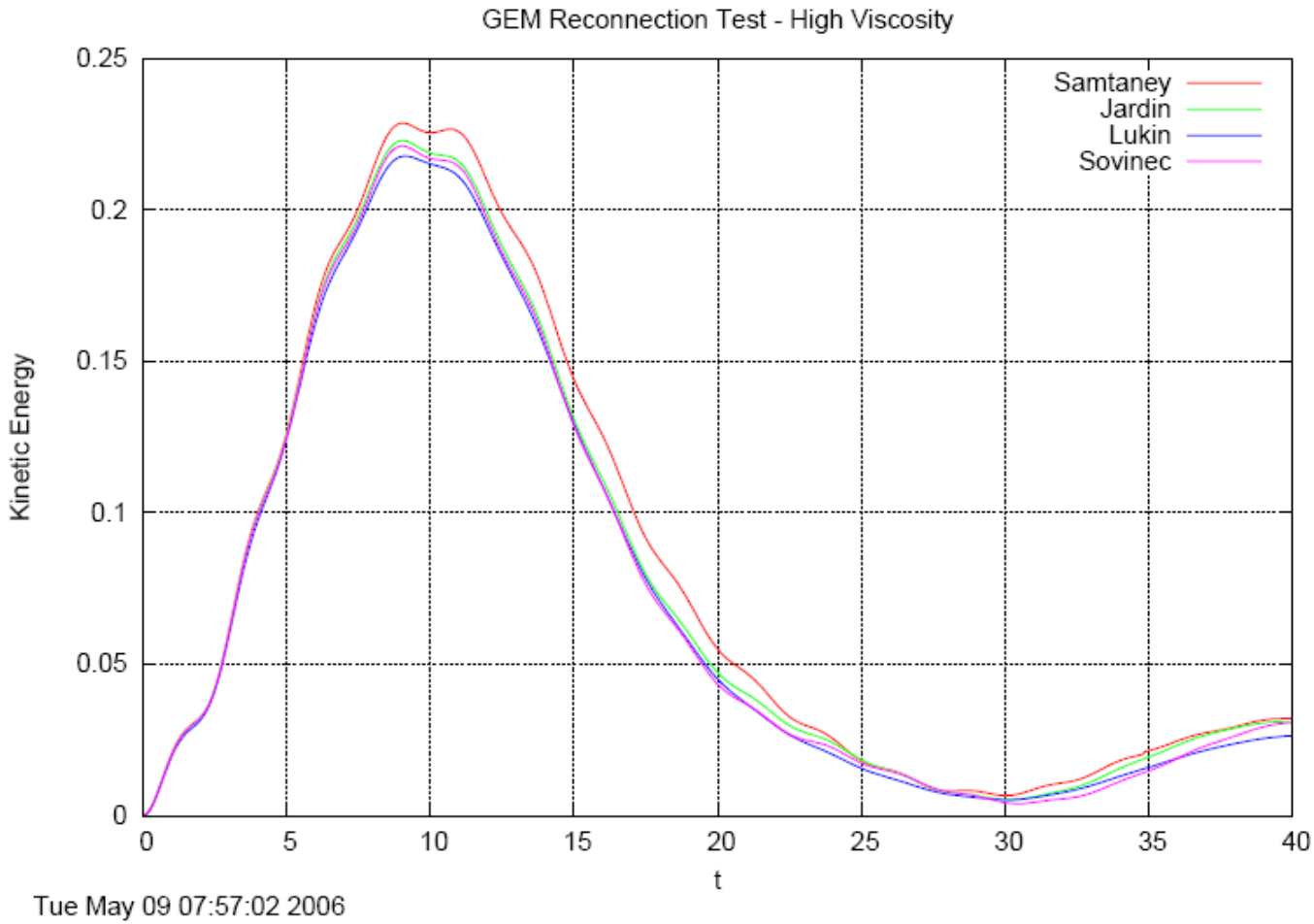

Comparison of kinetic energy vs time for M3D-C^1, NIMROD, Glasser/Lukin SE code, and Samtaney AMR code for GEM base case: η=0.005 , μ=0.05

Nonlinear Benchmark

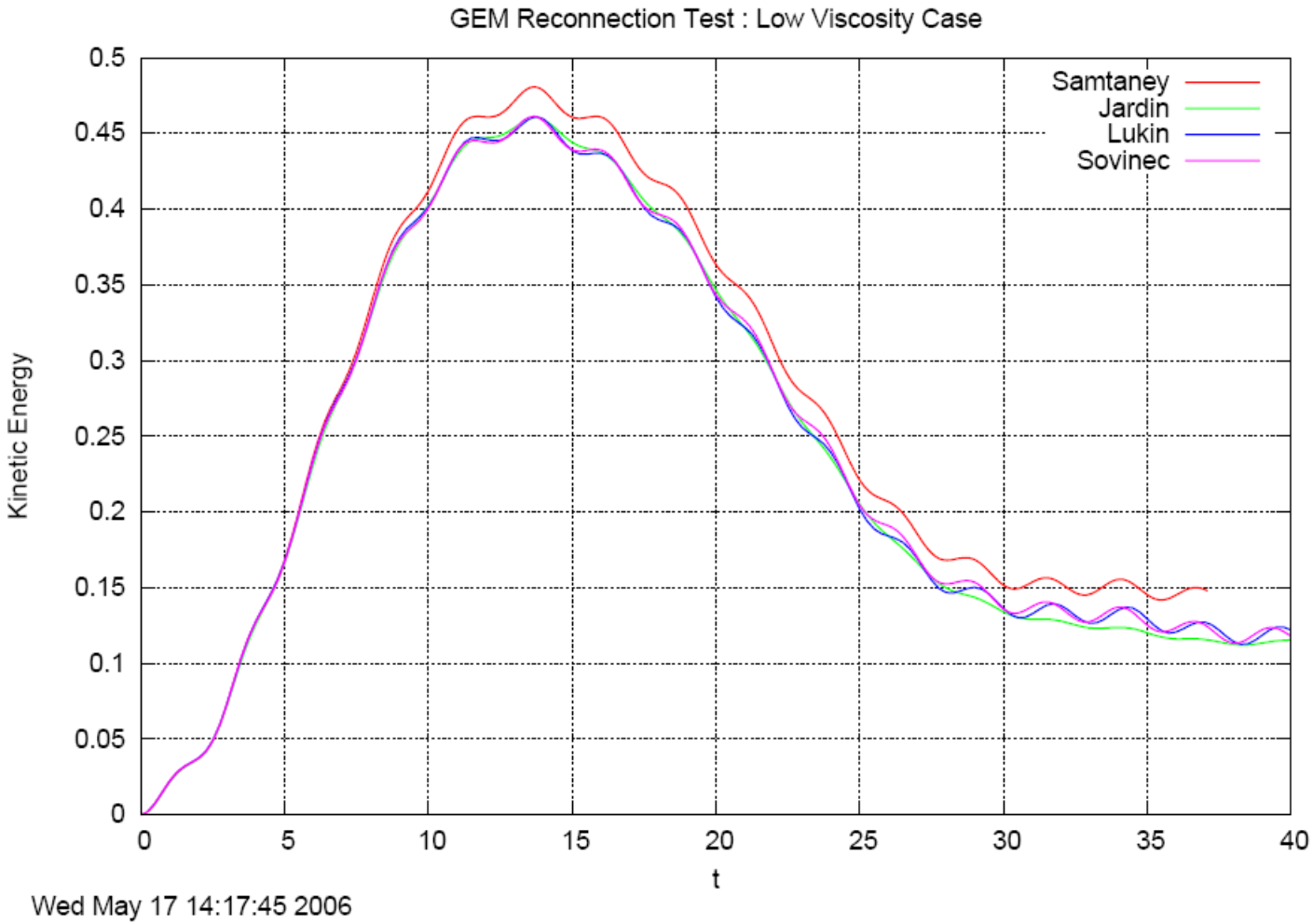

Comparison of kinetic energy vs time for M3D-C^1, NIMROD, Glasser/Lukin SE code, and Samtaney AMR code for GEM base case: η=0.005 , μ=0.0005

Nonlinear Benchmark

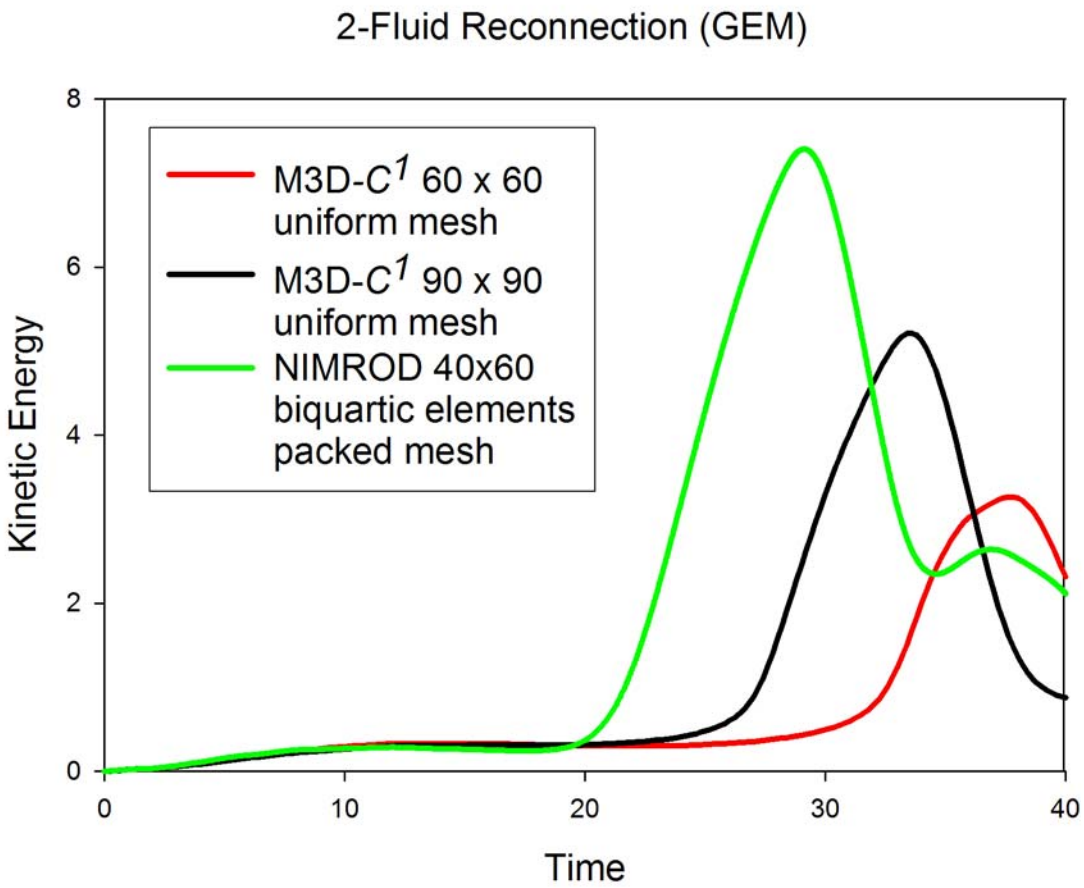

2-fluid benchmark comparisons are underway for GEM base case: η=0.005 , μ=0.05. For same parameters, kinetic energy is 10 times greater than for resistive MHD. Explosive growth in nonlinear phase requires high resolution.

Physics Studies-1 (Sawteeth)

- A campaign is underway to model the sawtooth behavior in a small tokamak (CDX-U).
  - Small tokamaks operate in regimes accessible to present day codes:
    - Resistive MHD: Current sheet thickness ~ $S^{-1/2}$
    - Two-fluid MHD: ion skin depth ~ $n^{-1/2}$
  - We are using this also as a non-trivial 3D nonlinear test problem for M3D and NIMROD
    - Verification and Validation
- These studies will later be extended to larger machines and to ITER geometry and parameters
  - Physics of the trigger and the crash time
  - Role of ballooning and other secondary instabilities
  - Physics of energetic particle stabilization
  - Interaction of MHD physics with RF physics (SWIM)

Progress in Sawtooth Studies

- Nonlinear MHD simulation with actual device parameters for CDX-U is capable of tracking evolution through repeated sawtooth reconnection cycles.

- M3D and NIMROD agree in linear mode structures

- High-n modes are stabilized by perpendicular thermal conductivity

- The nonlinear sawtooth simulations require high toroidal resolution: 48 planes (22 modes) is probably not sufficient

- Nonlinear comparisons are proceeding but are difficult because:
  - Both codes are probably under-resolved toroidally, and treat toroidal direction differently (spectral vs finite difference)
  - The n=0 equilibrium evolution is important for the sawtooth, and there are small differences in the way that M3D and NIMROD treat equilibrium sources which make big differences…these are being addressed.

- The parallel heat conduction model in M3D is yielding physical results

- Developed new elliptic solver for Cray X1E

Dynamic Relaxation in M3D for Cray X1E

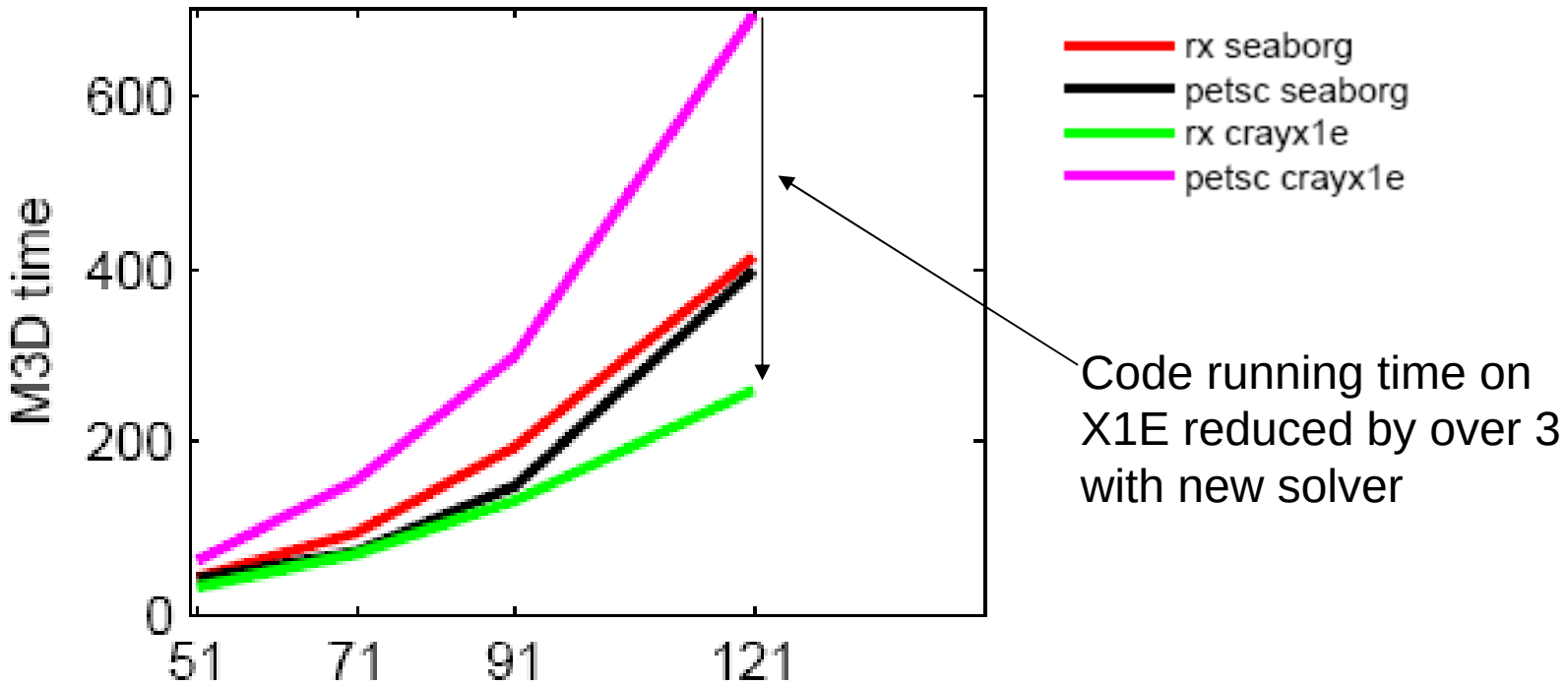

- The best PETSc solvers do not perform well on the Cray X1E:
- We developed and implemented a new elliptic solver for M3D called Dynamic Relaxation that performs much better on the X1E
- Could still be improved more, but X1E is now usable for M3D

CDX-U (From Stutman and Kaita, 1999?)

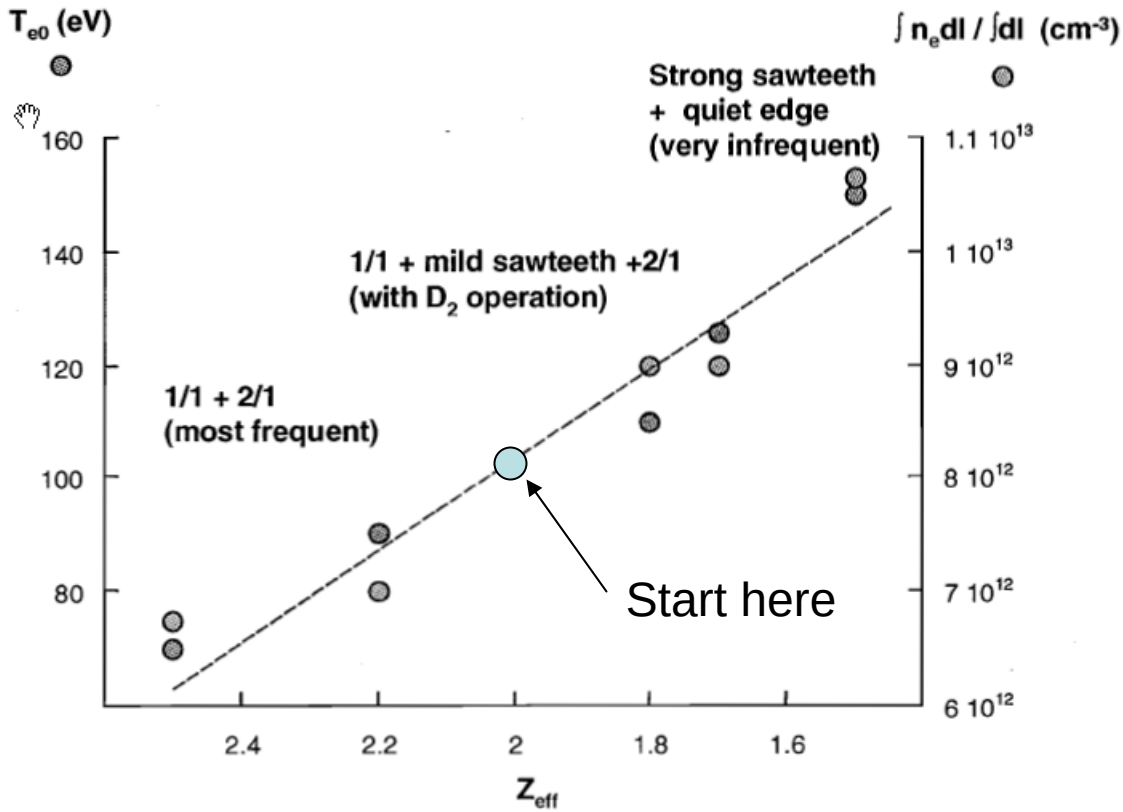

Other quantities obtained by fitting magnetics to TSC calculation. Goal is to benchmark codes, and then reproduce different MHD phenomena in different regimes

n=1 Eigenmode

Incompressible velocity stream function U

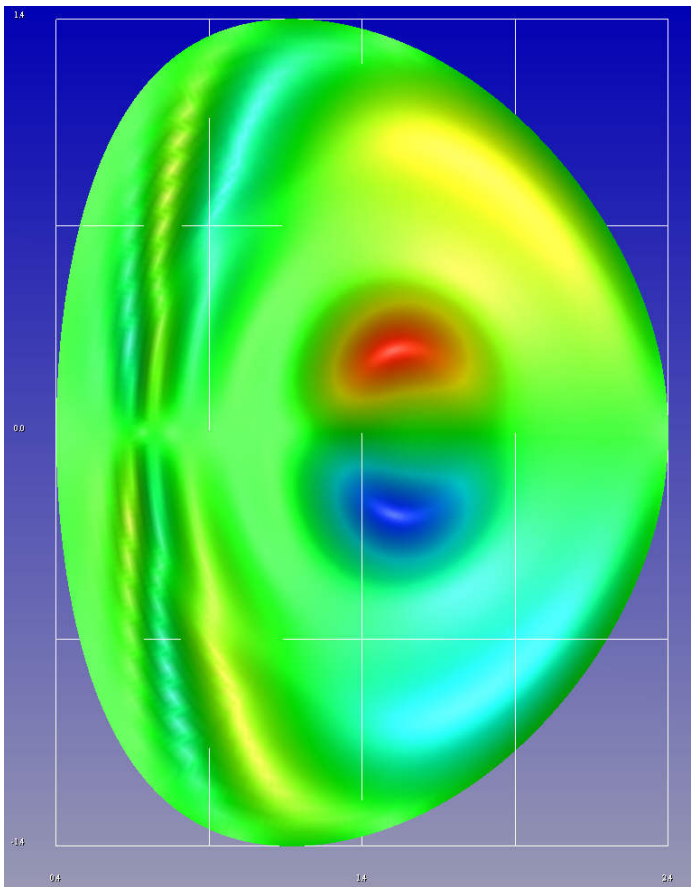

Toroidal current density J_ϕ

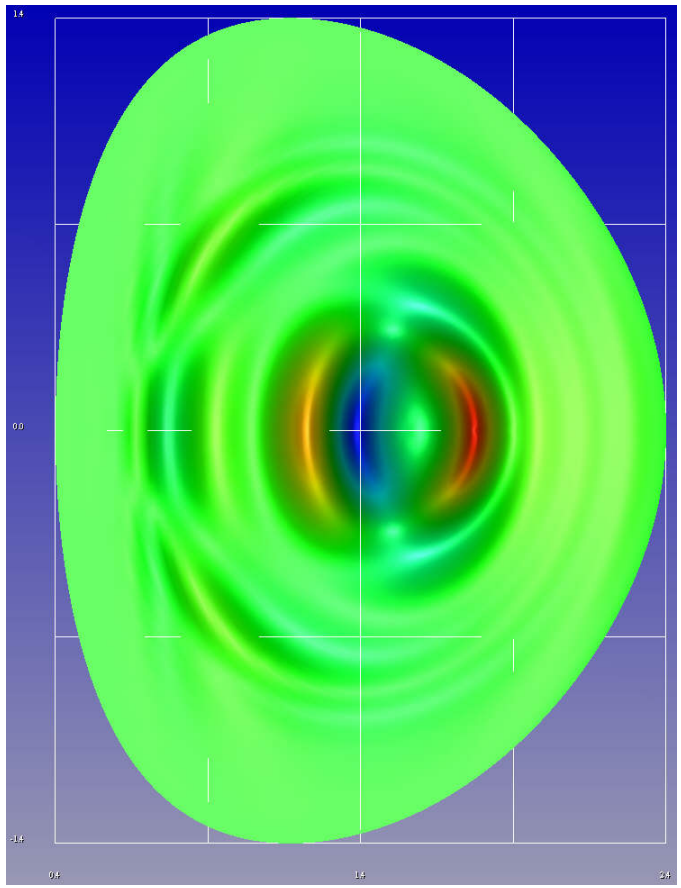

$\gamma \tau_A = 8.61 \times 10^{-3} \rightarrow$ growth time = 116 τ_A

Higher *n* Eigenmodes

Incompressible velocity
stream function U

$n = 2$

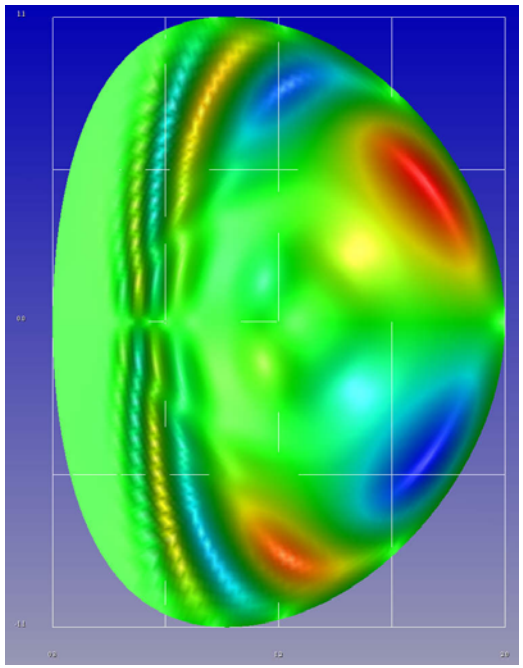

$m \geq 5$
$\gamma \tau_A = 1.28 \times 10^{-2}$

$n = 3$

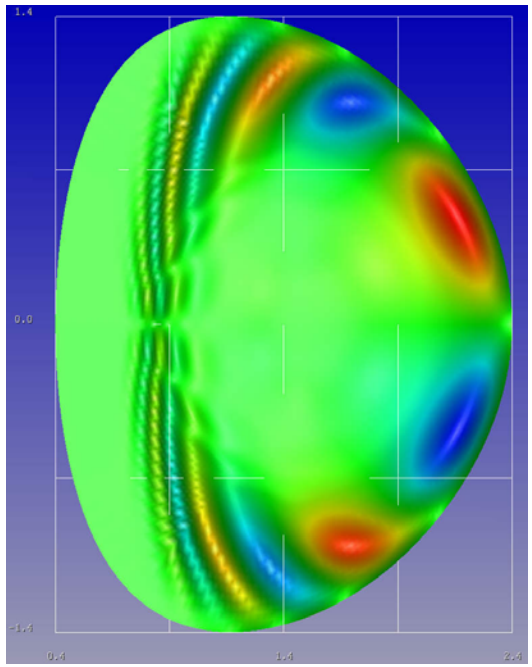

$m \geq 7$
$\gamma \tau_A = 1.71 \times 10^{-2}$

$n = 4$

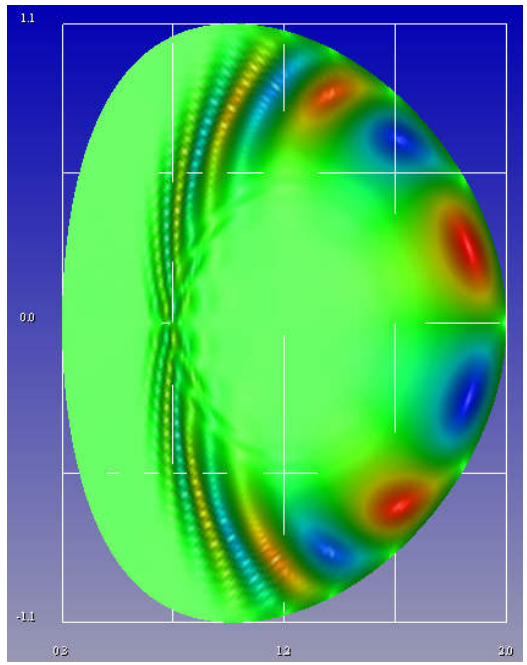

$m \approx 9$
$\gamma \tau_A = 1.87 \times 10^{-2}$

• • •

NIMROD and M3D agree in the Linear Eigenmode structures

NIMROD

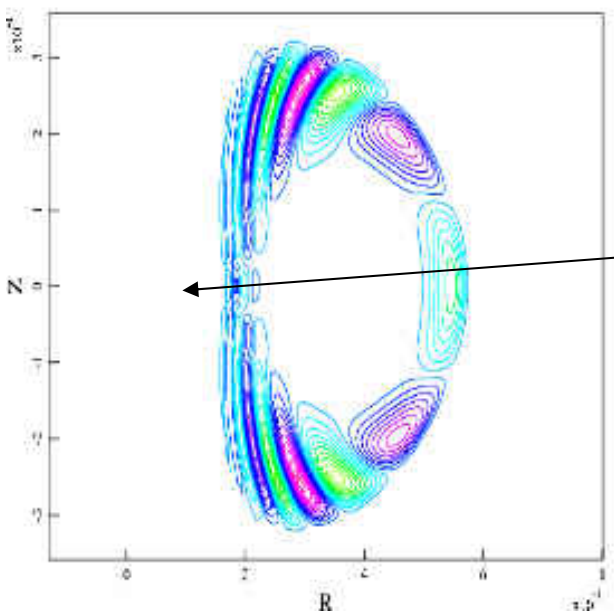

M3D

Incompressible velocity stream function U

$n = 3$

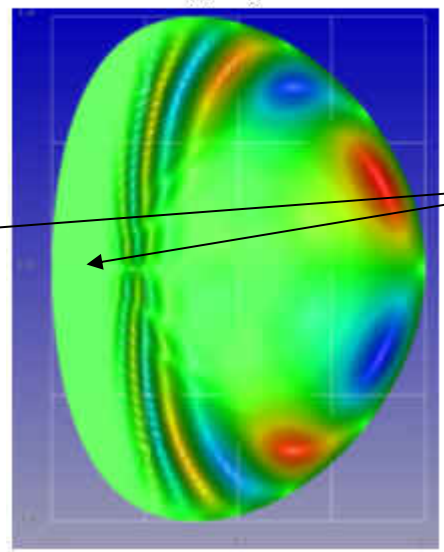

Note: mode amplitude completely vanishes in high-field side of torus

- Eigenfunctions for linear modes agree.
- Linear growth rates agree within a factor of 2 for all cases,
  - sensitive to exact form of dissipative terms.
- Nonlinear evolution sensitive to exact initial conditions and source terms for n=0 equilibrium.

High Perp. Heat Conduction Stabilizes All Ballooning Modes

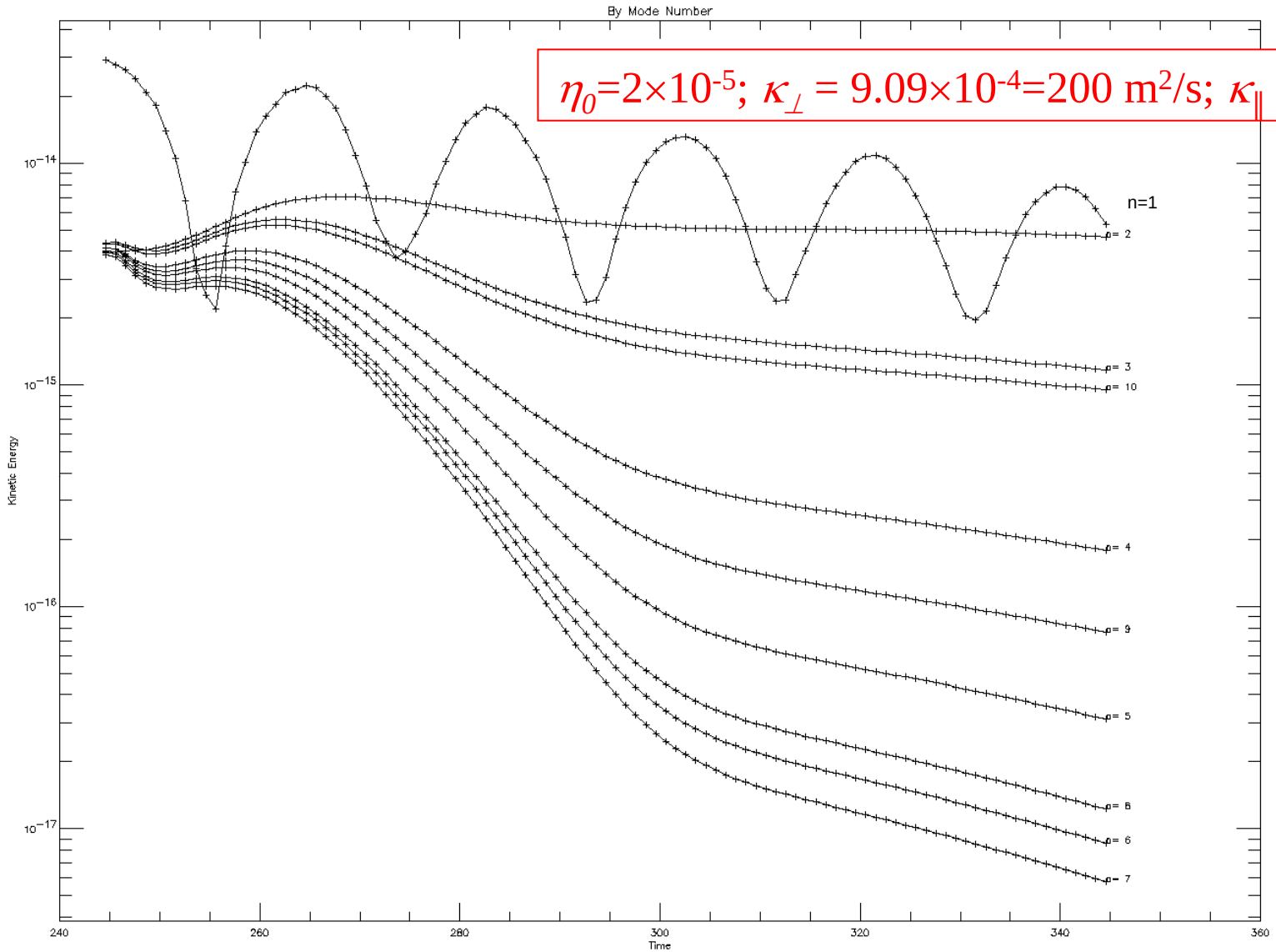

Breslau

Heat Conduction in M3D

Isotropic component in resistive MHD energy equation

$$\frac{\partial p}{\partial t} + \mathbf{v}\cdot\nabla p = -\gamma p \nabla\cdot\mathbf{v} + \rho\nabla\cdot\kappa_{\perp}\nabla\left(\frac{p}{\rho} - \frac{p_0}{\rho_0}\right) \qquad (1)$$

where p_0/ρ_0 is the equilibrium temperature.

Artificial sound wave model for $\kappa_{\parallel}$:

$$\frac{\partial T}{\partial t} = s\frac{\mathbf{B}\cdot\nabla u}{\rho} \qquad (2a)$$

$$\frac{\partial u}{\partial t} = s\mathbf{B}\cdot\nabla T + \nu\nabla^2 u \qquad (2b)$$

where s is the electron sound speed.

Test of Parallel Transport in M3D

Solving (2) only, holding other quantities fixed, with $s = 6\ v_A$.
Start from equilibrium temperature distribution, with field as shown for t = 1795.61 below.

Poincaré plot

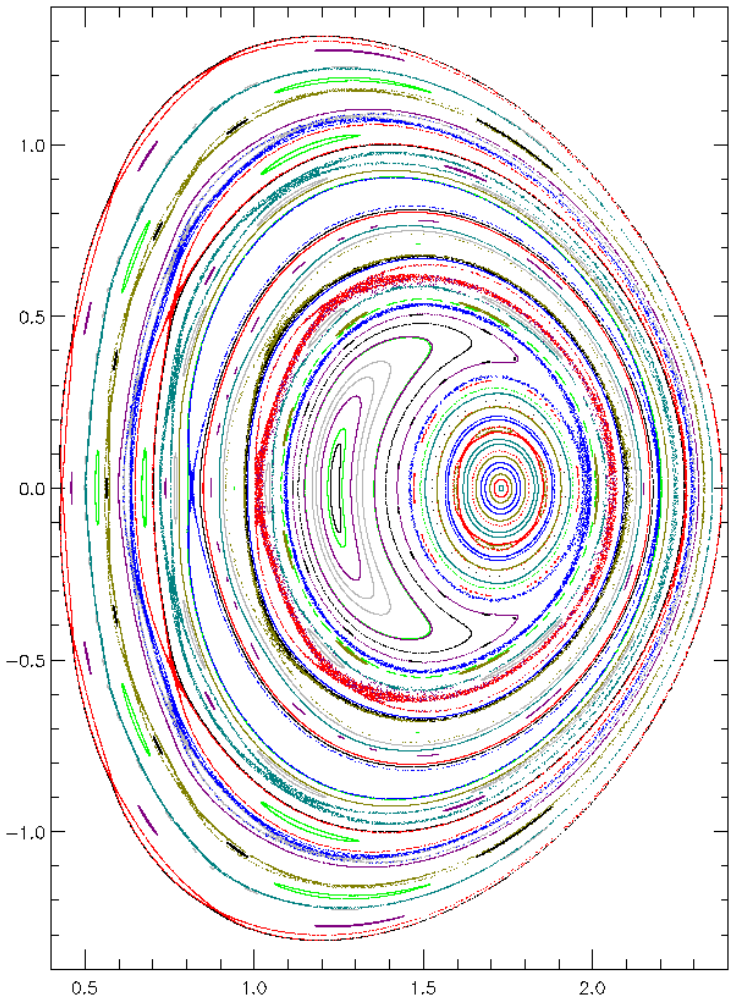

t = 1795.61

T, Surface plot, ϕ=0

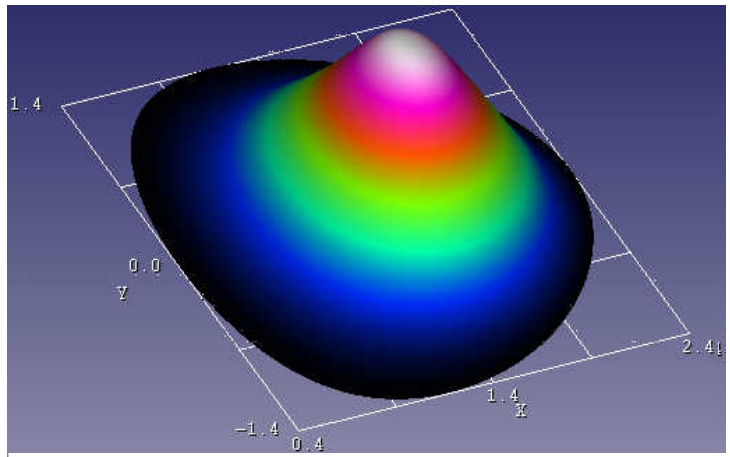

T, midplane cross-section

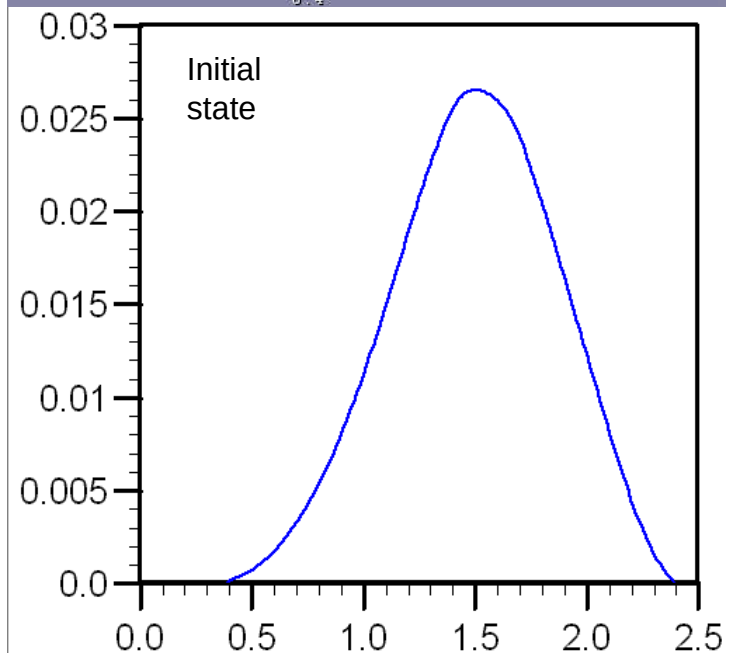

Breslau and Hudson

Parallel + Perpendicular Transport

• Parallel heat conduction alone results in very fast equilibration, but does not rapidly smooth out all bumps where field is stochastic.

• Adding some $\kappa_\perp$ and solving (1) as well as (2) can quickly smooth the smallest bumps:

continue, setting
$\kappa_\perp = 10^{-4}$ (22 m^2/s)

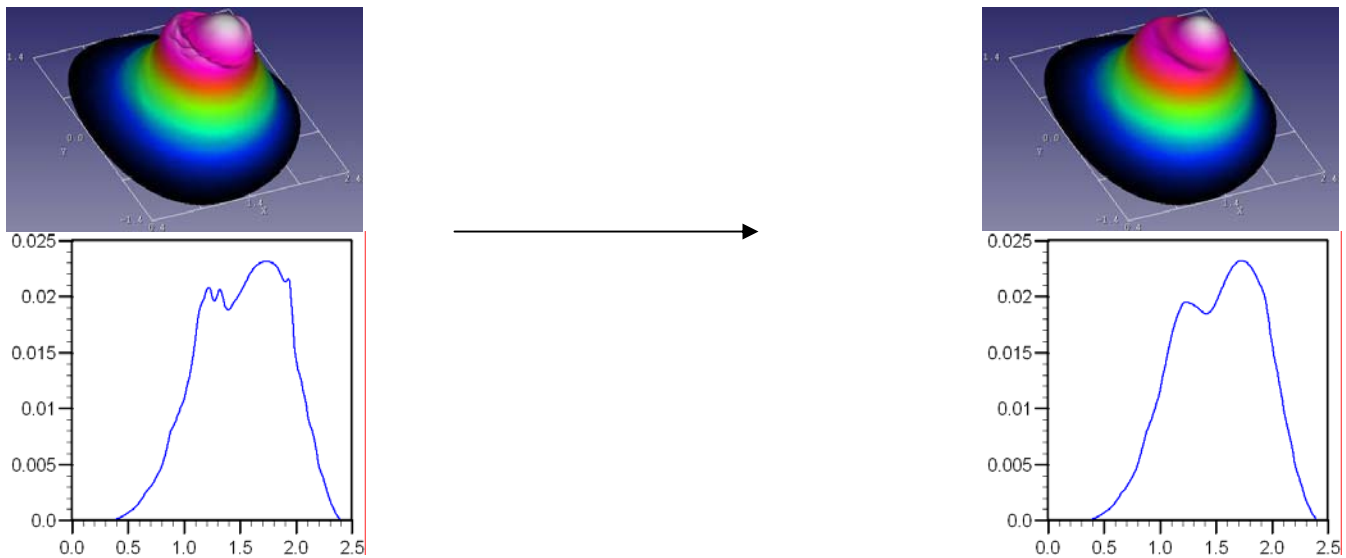

Breslau and Hudson

Nonlinear Sawtooth History

10 Modes Retained (24 planes)

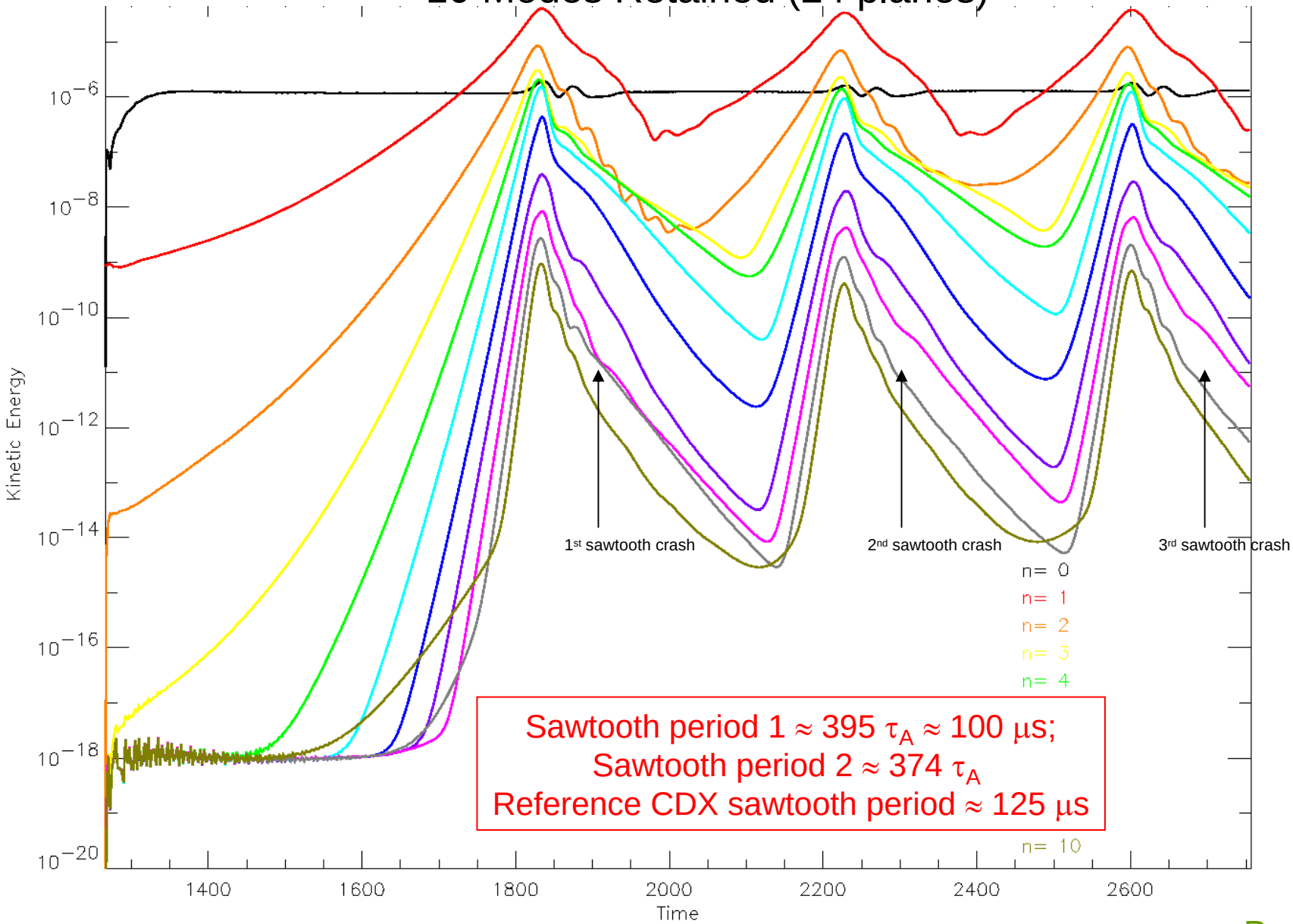

Breslau

Total Energy and Core Temperature

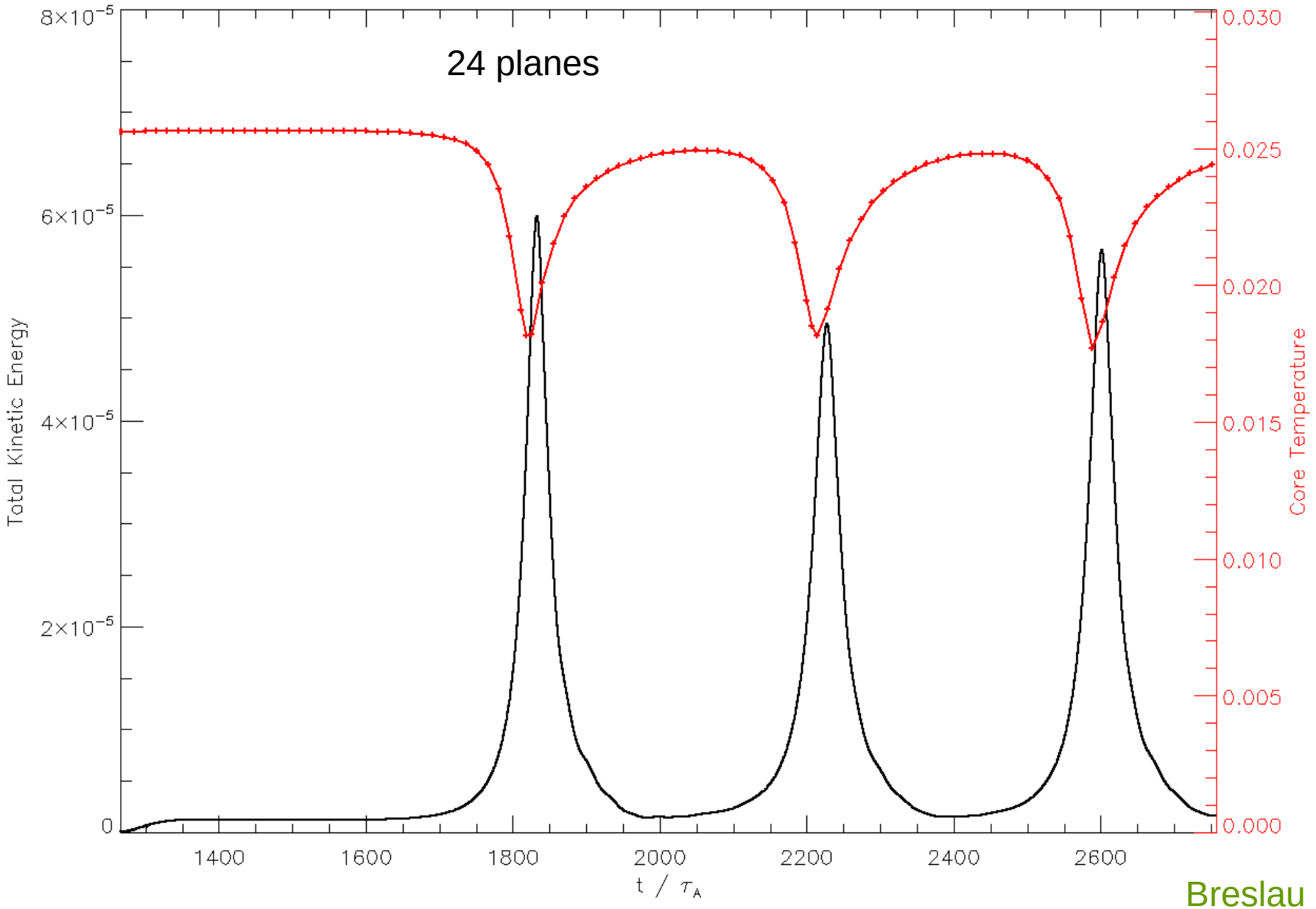

Breslau

Flux surfaces recovered: t = 2094.08

Poincaré plot

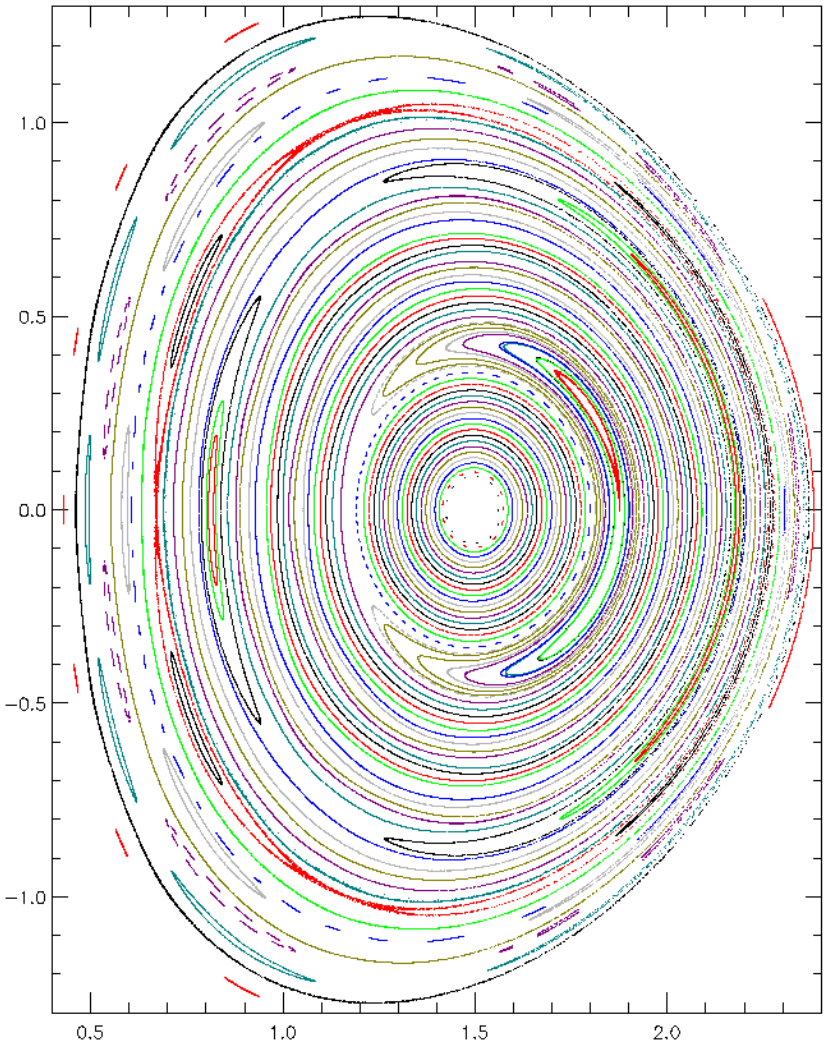

Temperature profile

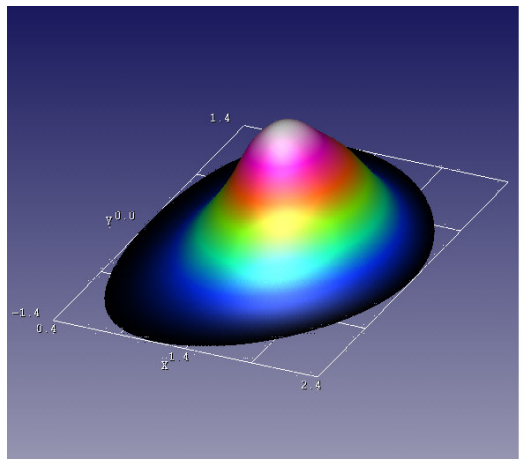

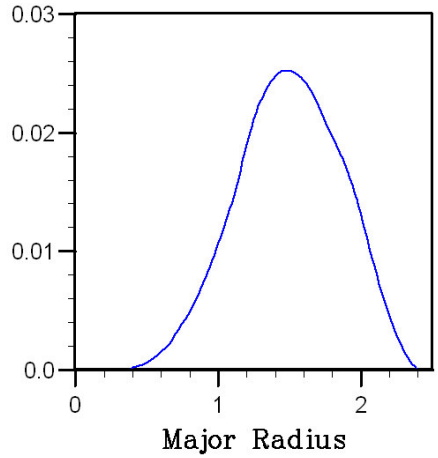

q profile

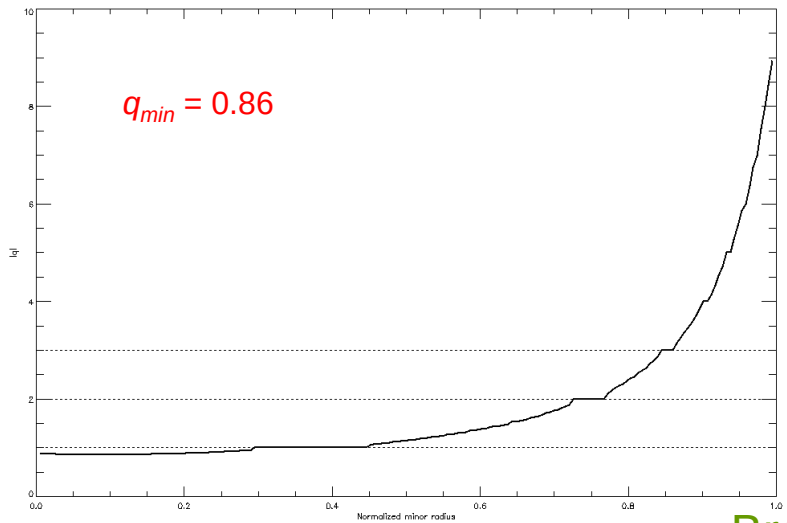

Breslau

Nonlinear Sawtooth History

22 Modes Retained (48 planes)

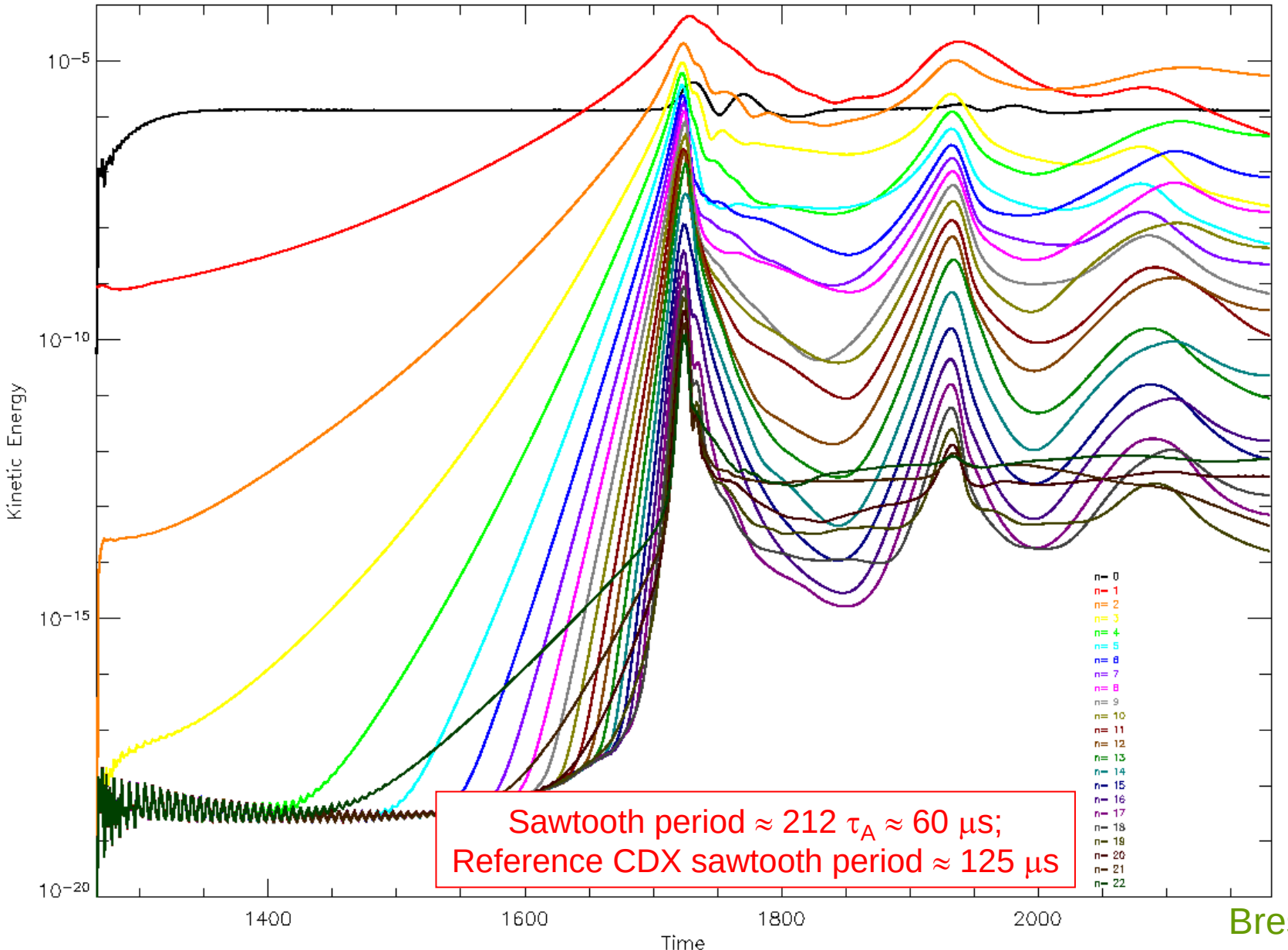

Breslau

Total Energy and Core Temperature

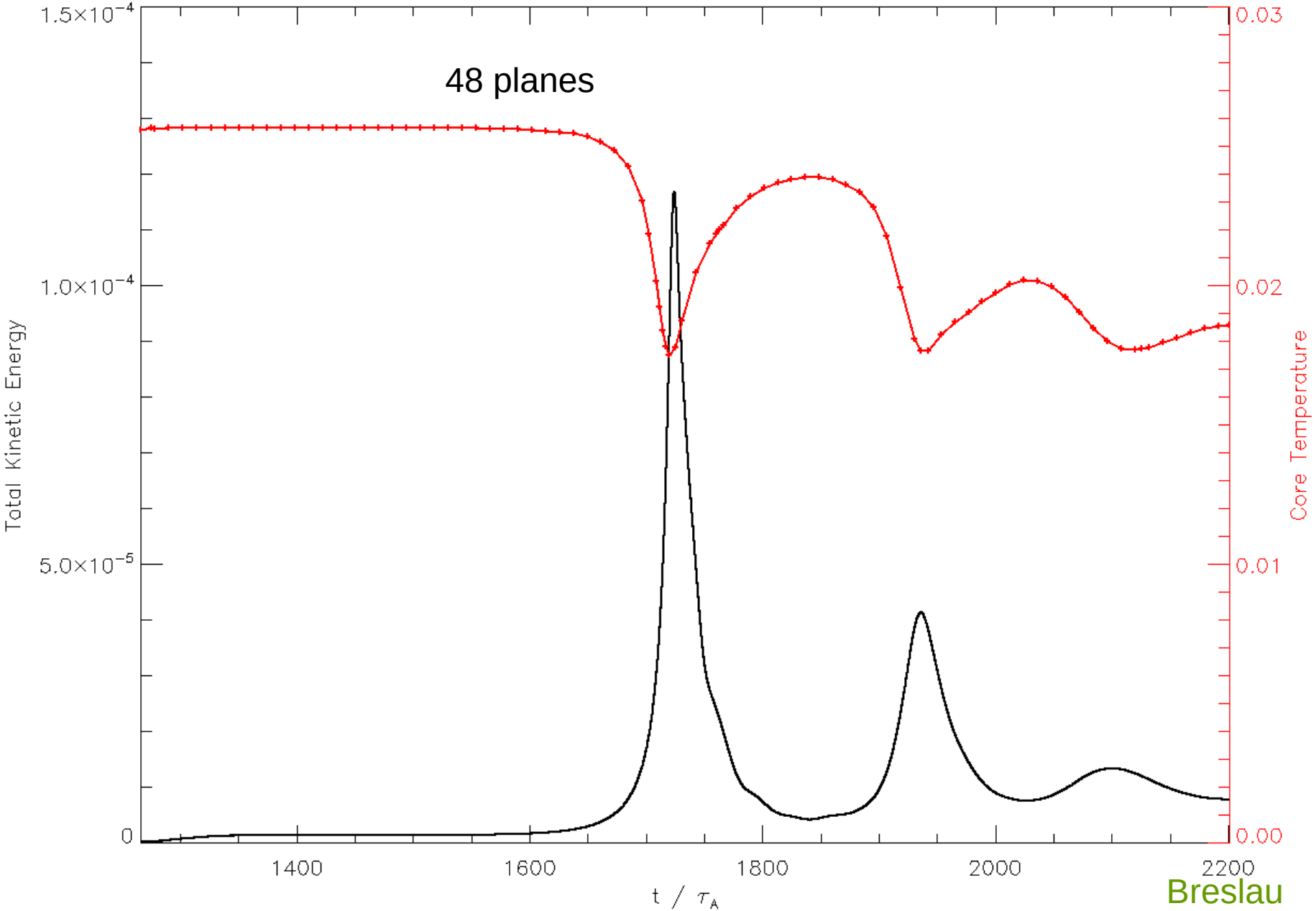

Breslau

Lack of Convergence in Toroidal Resolution

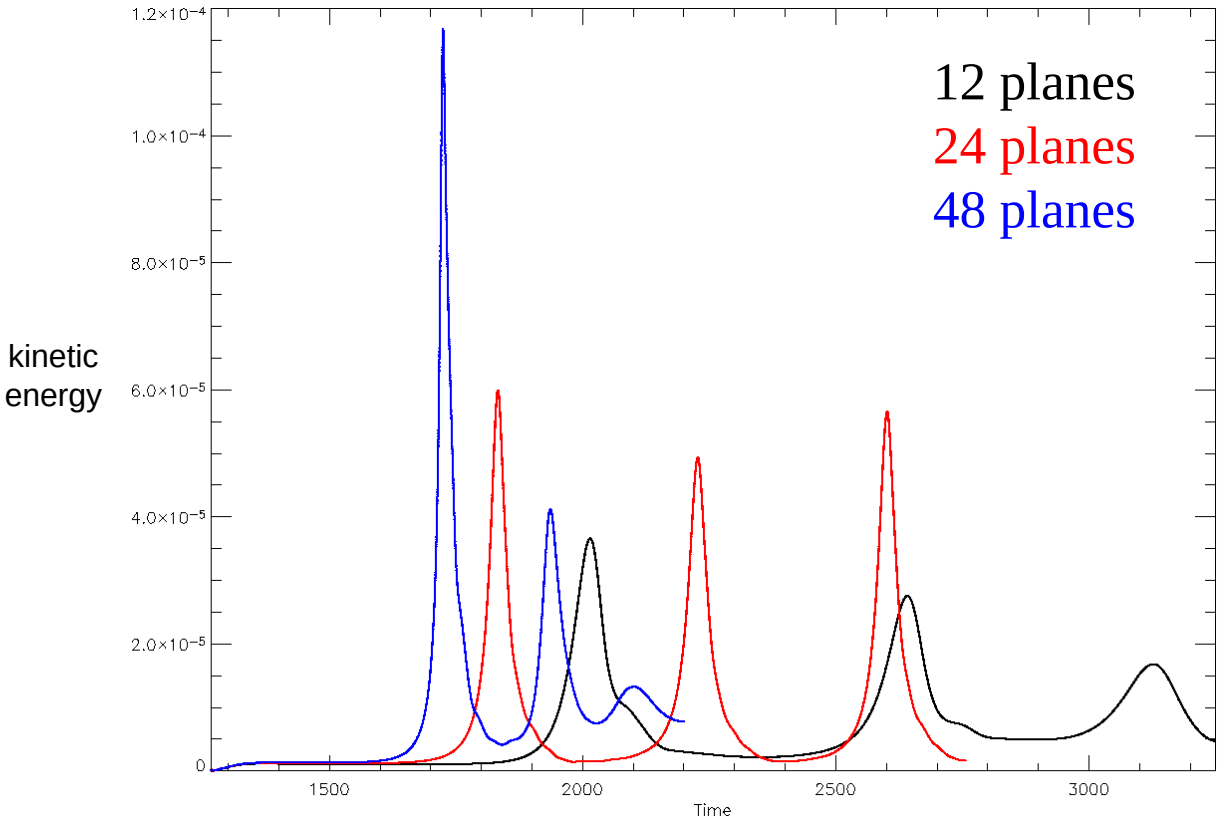

- Both timing and energy of peaks are different.
- Outer flux surfaces do not heal in highest-resolution case.

- Energy in higher-*n* modes significantly affects sawtooth evolution.
- Further study is needed to assess convergence on this case.

Breslau

Toroidal Structure of the Sawtooth Current Sheet

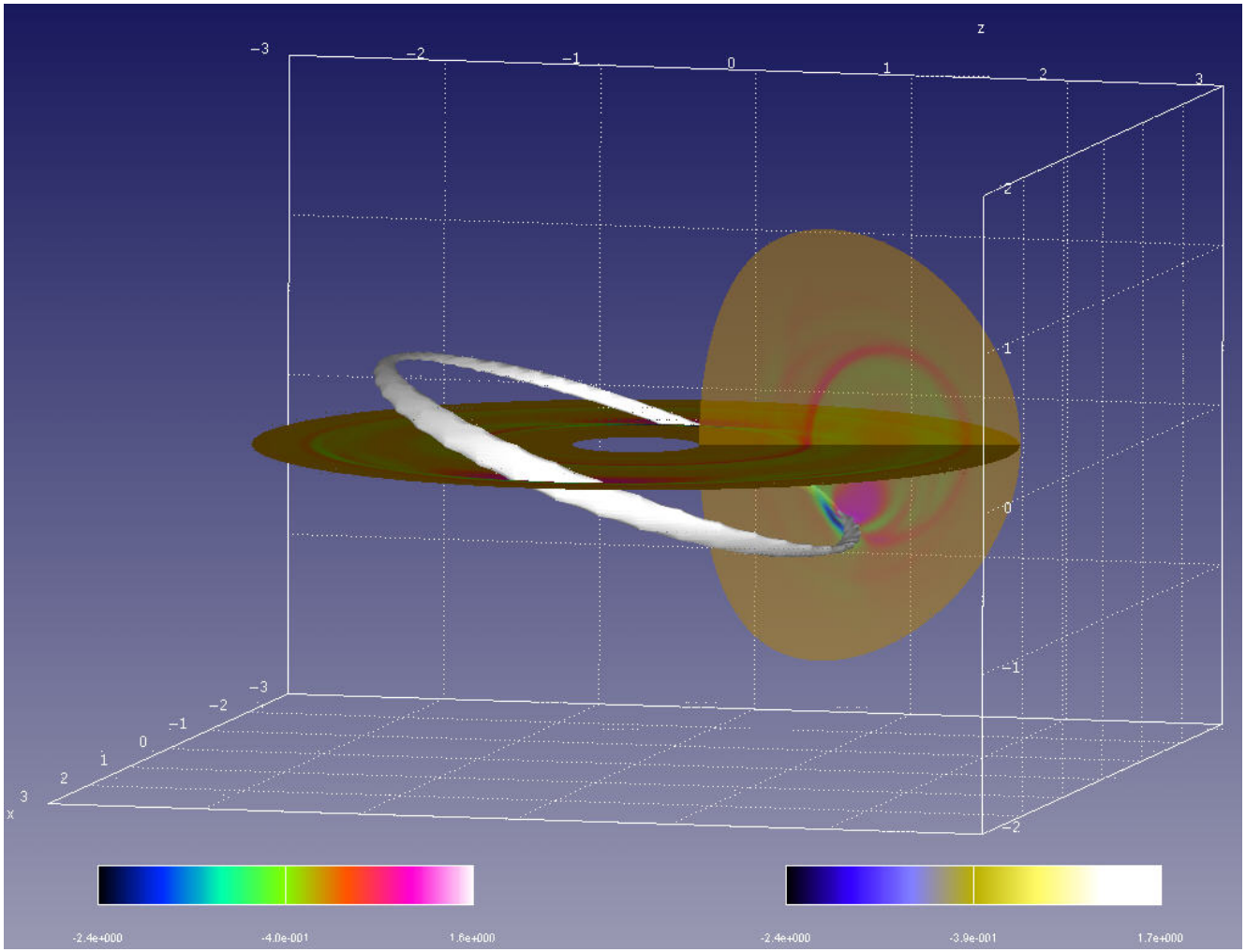

Isosurface of n>0 part of toroidal current density during sawtooth crash shows that the current peak occurs where the 1,1 island is reconnecting. Following this peak around the torus indicates that its variation in ϕ may not be fully resolved in this calculation.

Breslau

Toroidal Structure of the Sawtooth Current Sheet, continued

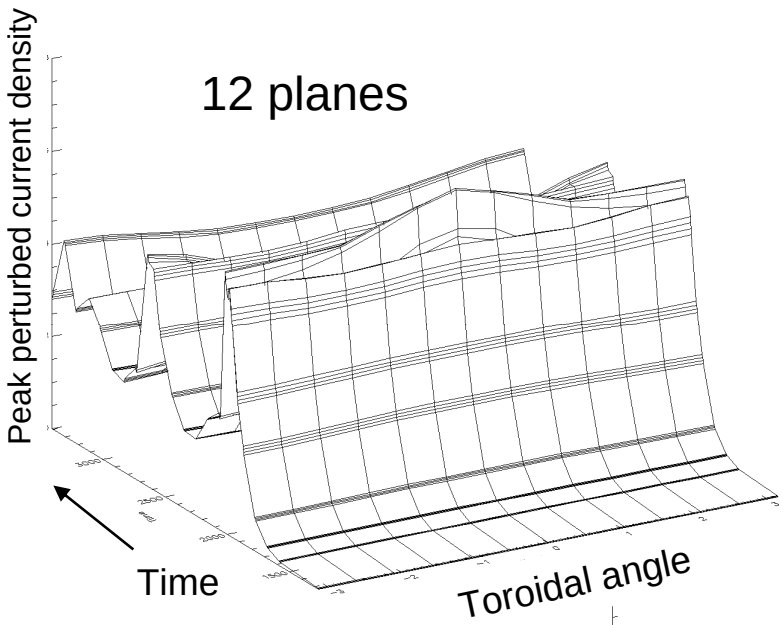

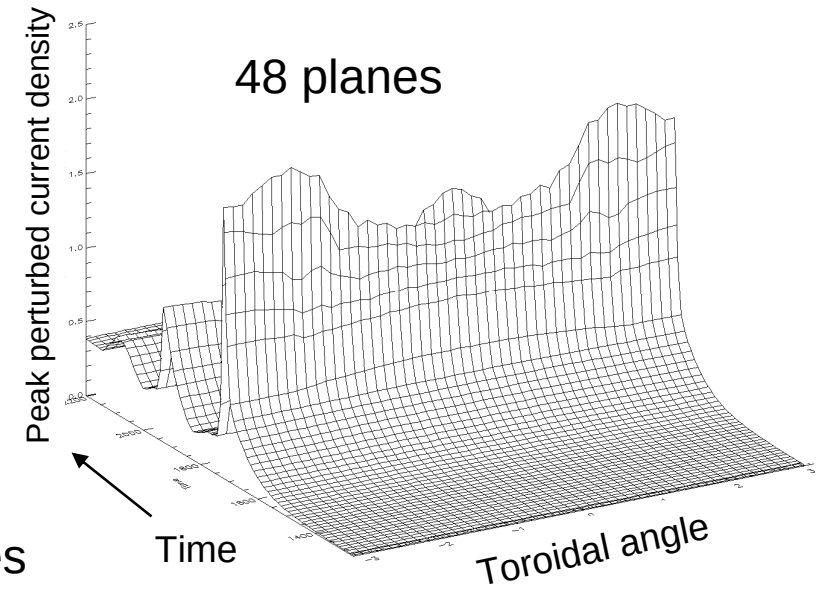

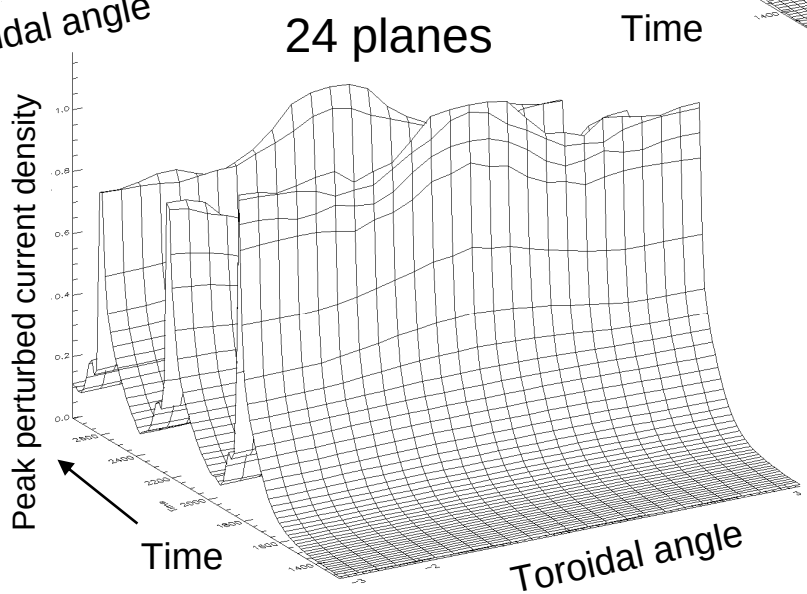

Breslau

Physics Studies-2 (ELMs)

- Exploratory studies are underway to understand many poorly understood features of Edge Localized Modes (ELMs)
  - Explanation of the ELM trigger
  - Dependence on velocity shear
  - Dependence on Toroidal field strength (ρ^*)
  - What sets the ELM type and frequency

- As we understand these better, and our predictive capability increases we will
  - Predict what kind of ELM behavior is expected in ITER, and where are the heat and particles deposited
  - What external mechanisms, such as pellet injection, RF current drive, or boundary modulation are effective in modifying the ELM frequency
  - Can we improve the heuristic models that are implemented in the global transport models?

Progress in ELM Studies:

- Showed that flow shear reduces the (nonlinear) radial propagation of the mode even though it has relatively little effect on the linear modes
- Demonstrated that differences in the peak of the linear spectrum causes differences in the nonlinear growth, and that the nonlinear modes are driven where the linear modes peak
- Successfully calculated an entire ELM event to re-symmetrization (without density evolution)
- Developed a generalized up-wind method (for linear elements) to avoid negative densities during ELM crash.
- “2-fluid” terms effect linear mode growth, but do not appear to be important nonlinearly
- Initial ITER ELM studies for code comparison studies.

DIII-D has suggested that we do a comparative study of two ELMing discharges

113207- (B_T=2.1 ,low ρ^*)
113317- (B_T=1.0 ,high ρ^*)

Little difference in q

Deeper pedestal at lower B.

Both higher density and temperature at higher B.

Flow imposed for comparison.

Little difference in ω_*, therefore expect linear spectrum with two fluid to have similar differences to single fluid.

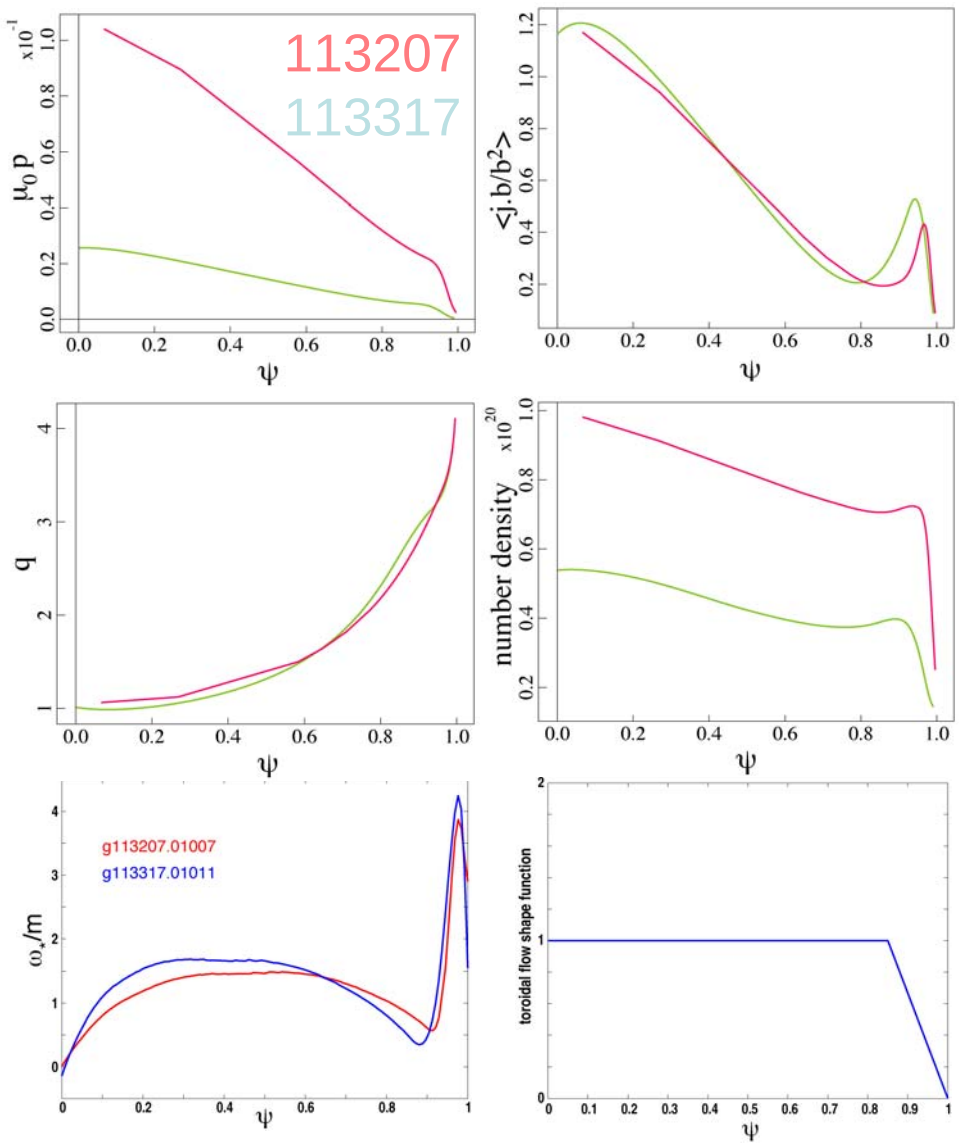

Difference in peak of linear spectrum causes difference in nonlinear growth

Higher linear growth in 113207 (high B)

Higher linear growth case peaks at higher n in linear spectrum.

ELITE results show peaking at higher n~20-40

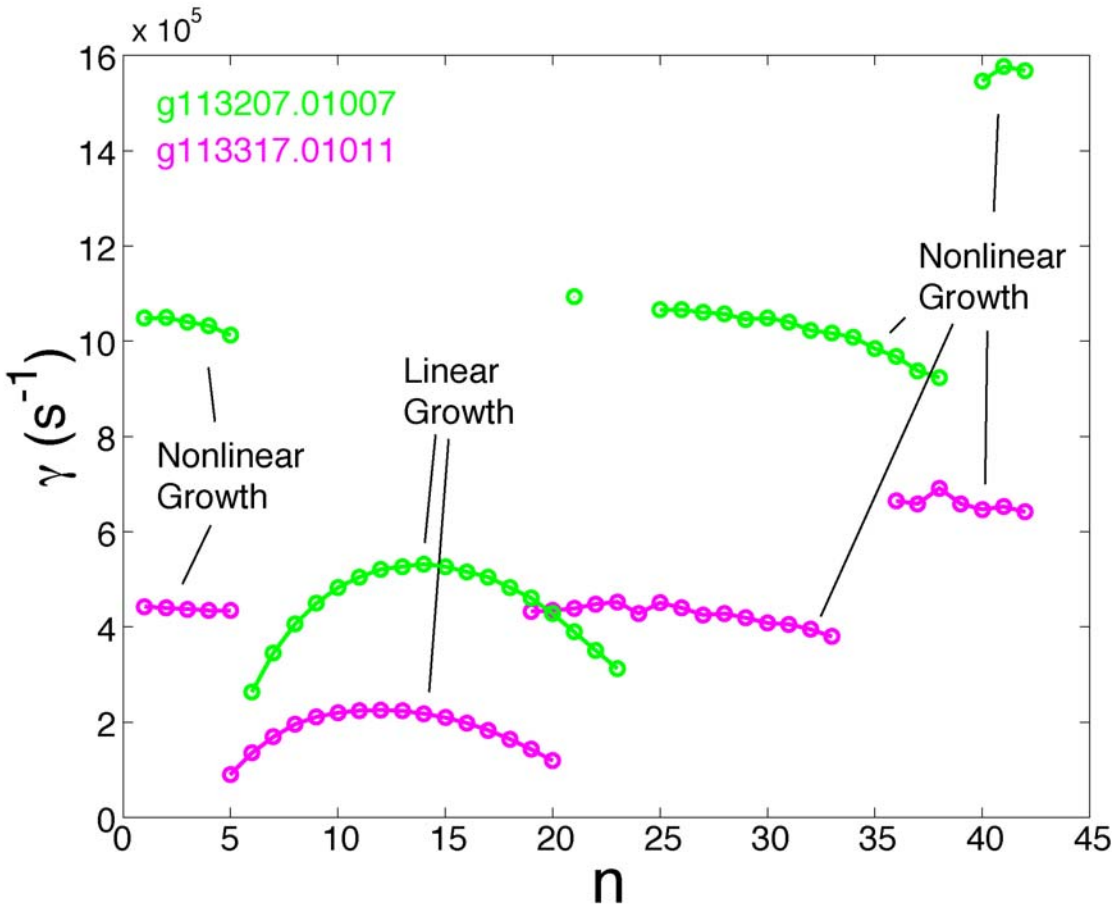

Brennan

With flow shear the mode structure is limited in radial propagation

Loss of energy similar in both cases.

Lower amplitude poloidal fluctuation and reduced radial gradients with flow shear.

Possible healing.

Subtle differences between two experimental cases under investigation.

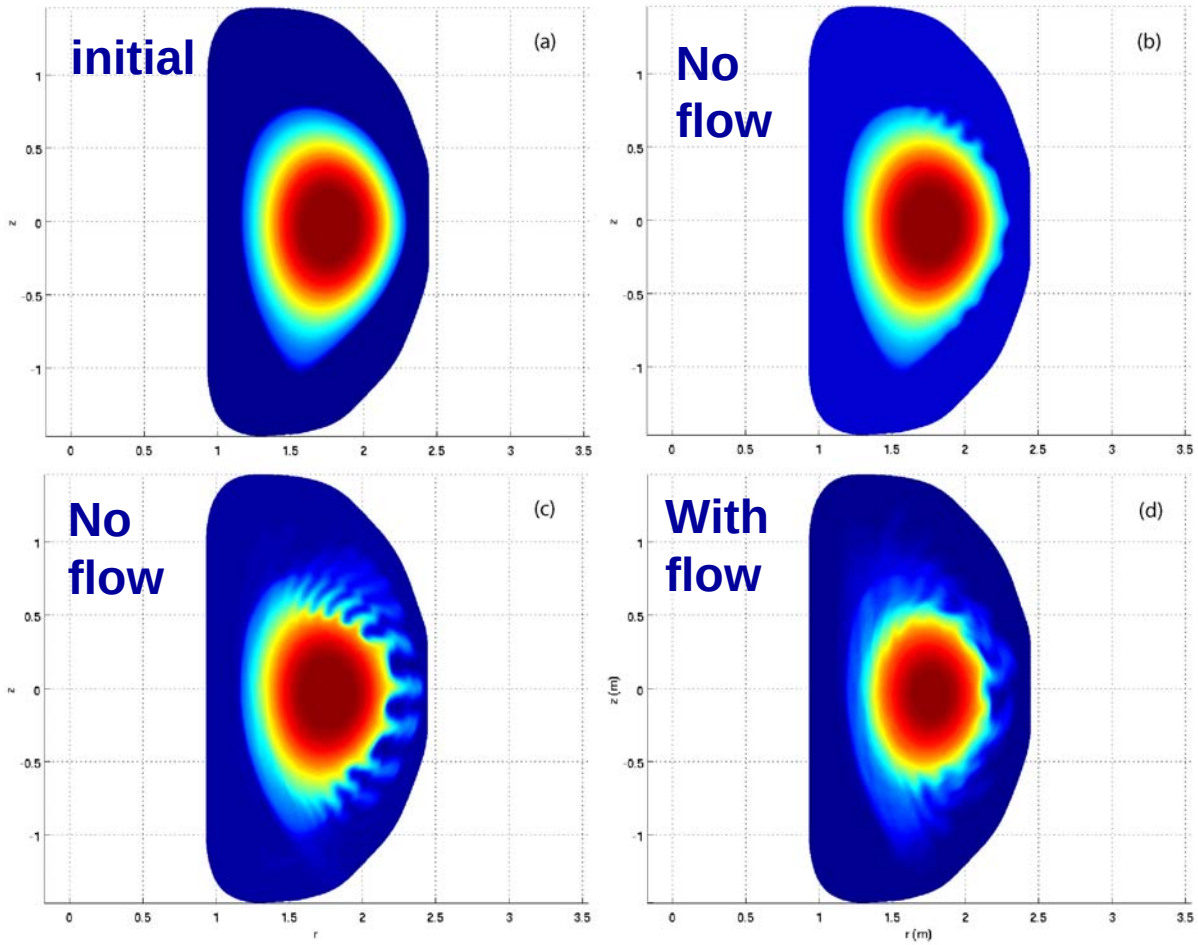

Brennan

Computation terminates with negative density despite large vacuum density

This occurs even with flow and seemingly smaller perturbations.

This happens despite large density in the vacuum which extends from the edge density in equilibrium.

Filamentary structures cause drops in density between them.

Investigating solutions.

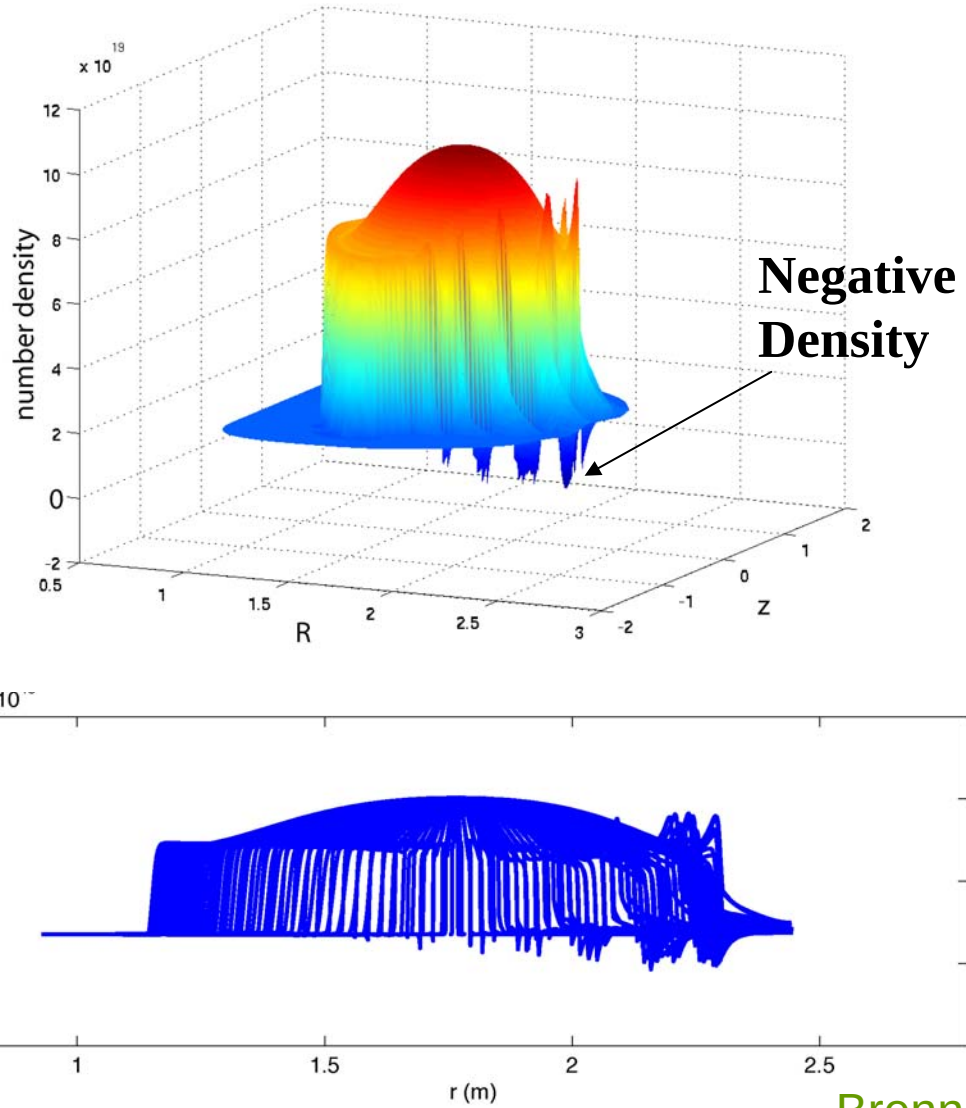

Brennan

g086166 DIIID ELM

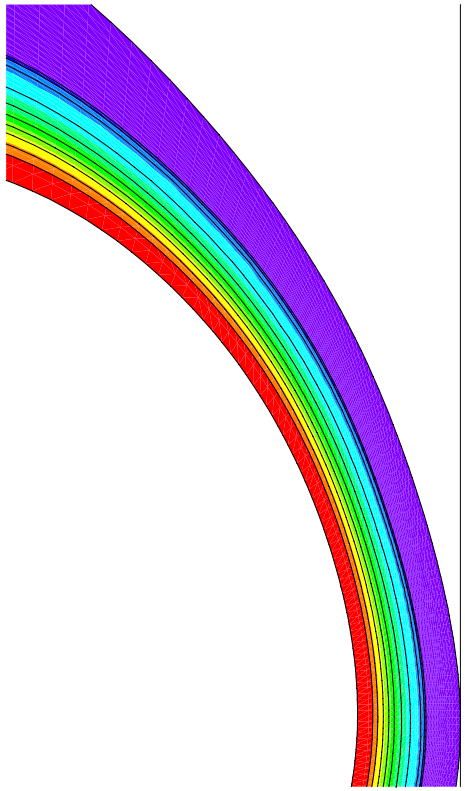

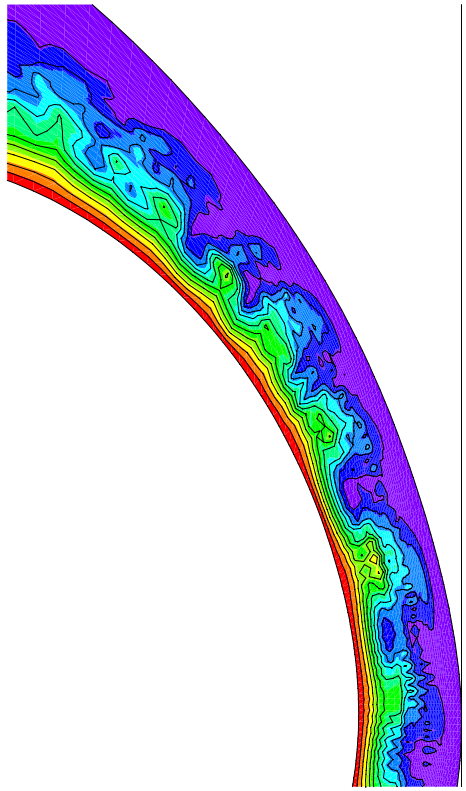

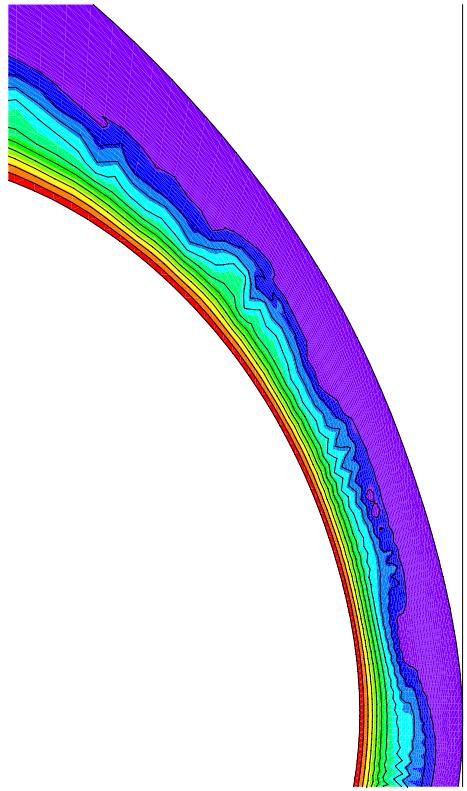

t = 27

Initial p

t = 67

ELM

t = 106

relaxation

M3D

Strauss

ITER mesh

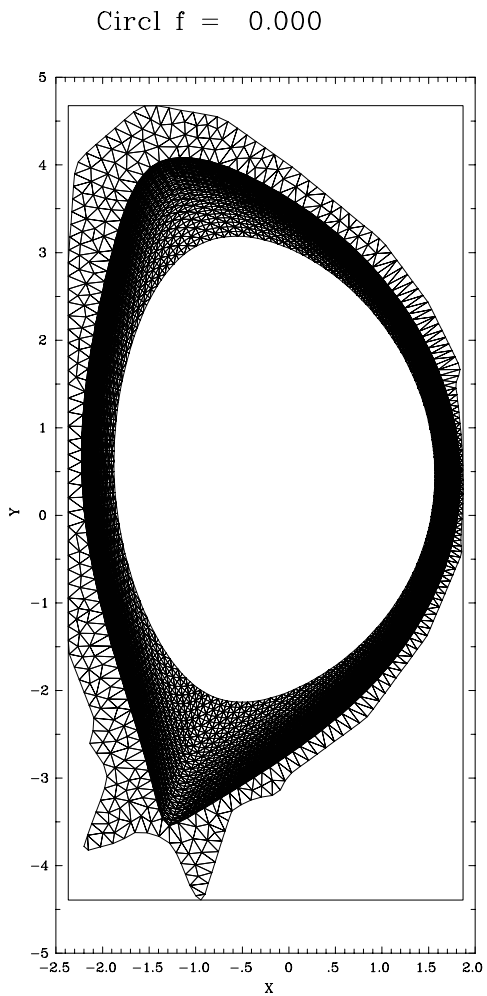

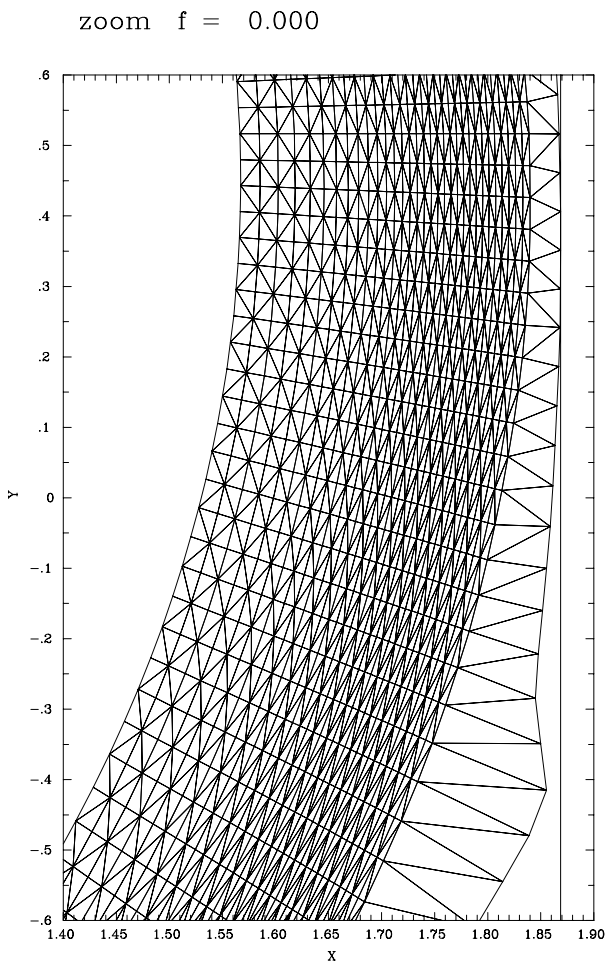

Strauss

ITER ELM: pressure time evolution

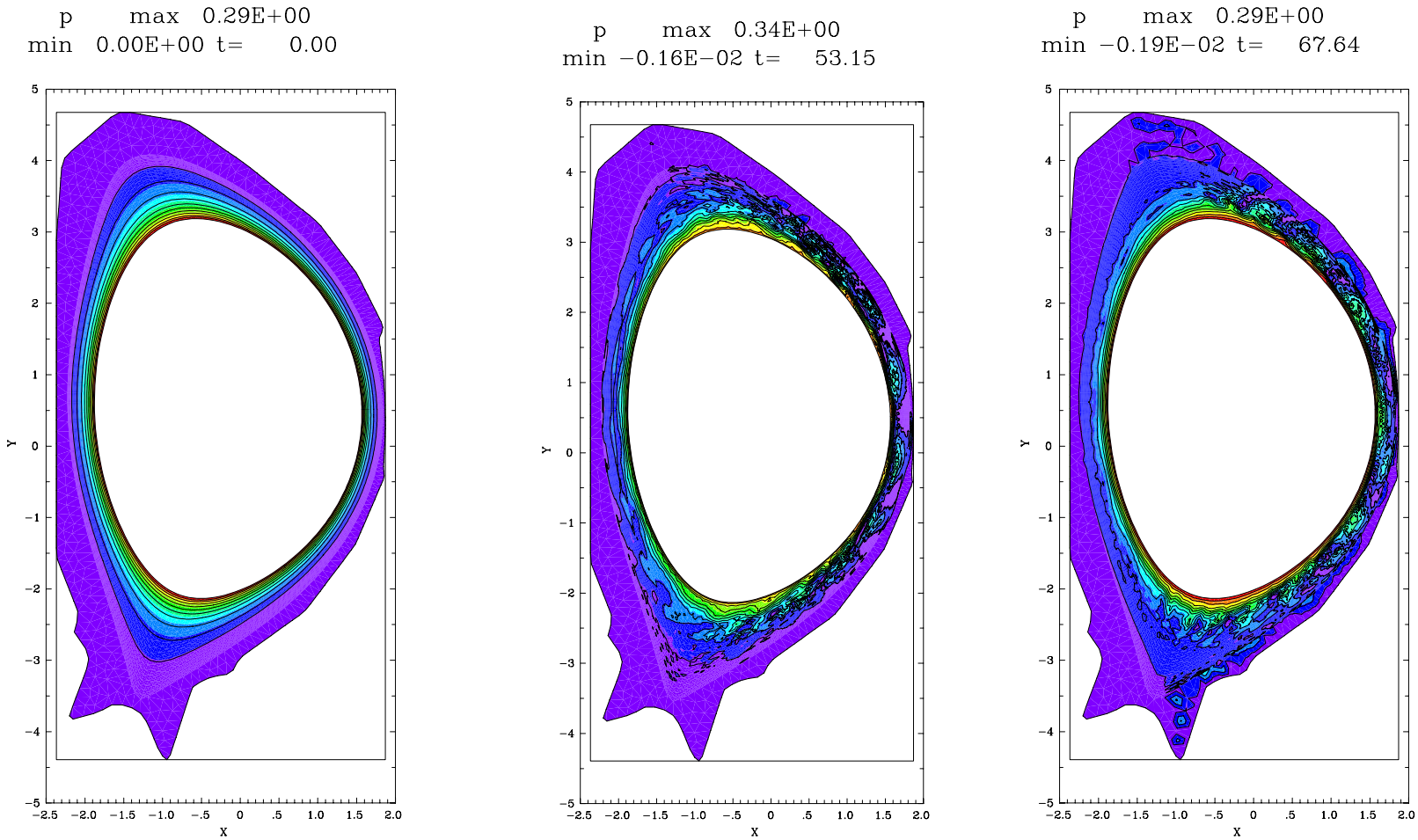

Strauss

ELM pressure: initial, mode growth, outflow

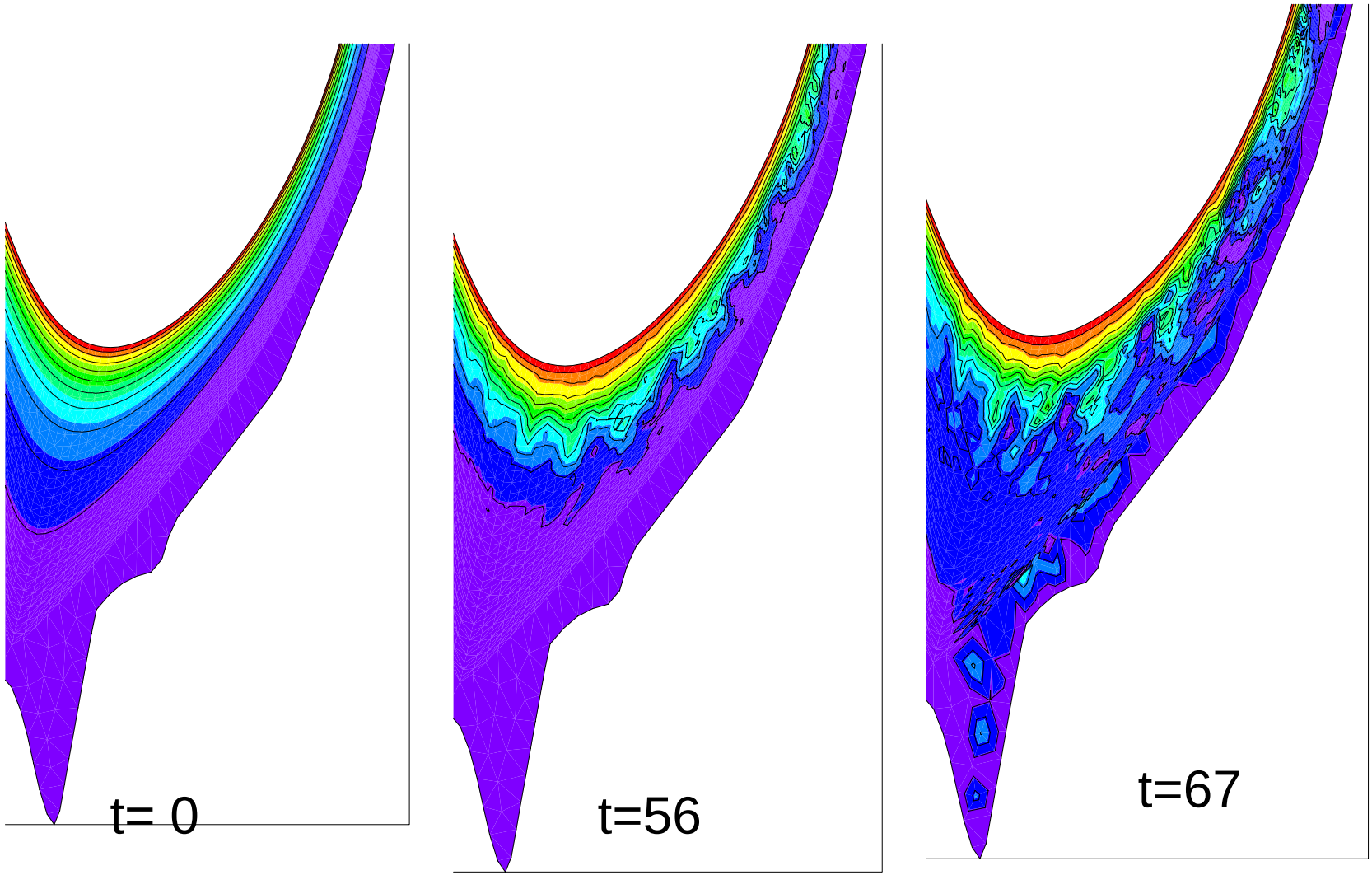

Strauss

ITER – pressure profiles initial, ELM crash, relaxation

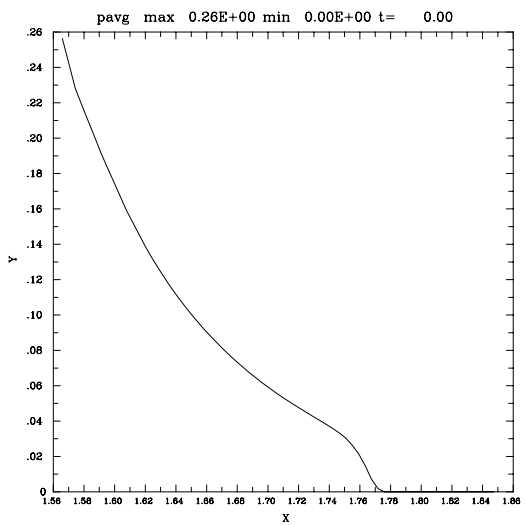

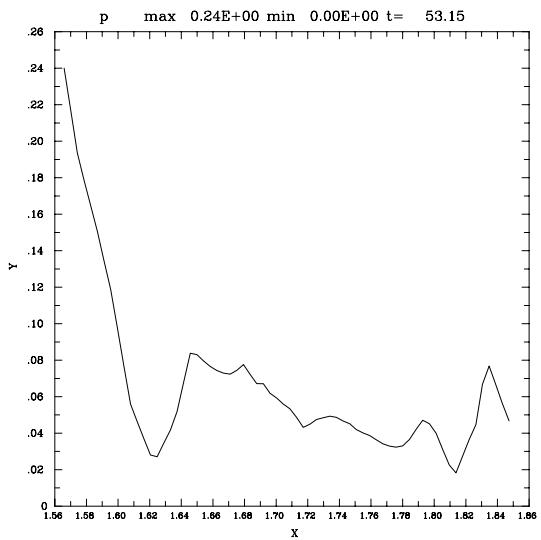

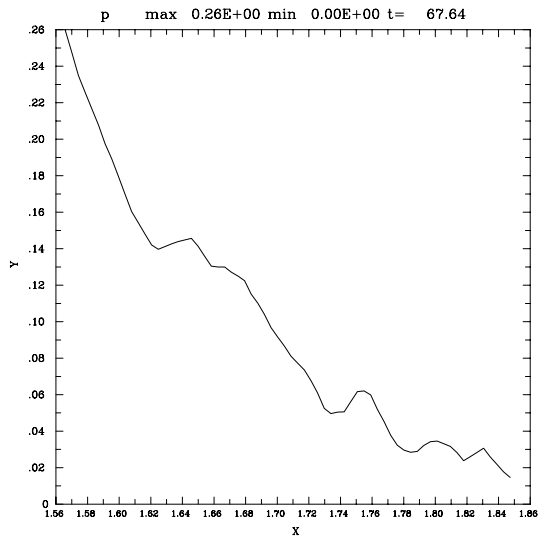

Strauss

Physics Studies-3 (Energetic Particle Modes)

- Basic physics studies are being performed of the effect of energetic particle (and kinetic thermal particles) on MHD modes
  - Relation between the internal kink mode and fishbone
  - Effect of plasma shaping on energetic particle modes
  - Nonlinear saturation of energetic particle modes
  - Effect of treating ions kinetically on MHD modes

- Goal is to develop a quantitative predictive model for a burning plasma
  - Effect of α-particles on internal kink (sawtooth) and other modes
  - Under what conditions will a significant fraction of the α-particles be lost before they thermalize

Progress in Energetic Particle Mode Physics

- M3D, NIMROD, and NOVA2 code agree for linear mode structure and growth rates
- Simulations of beam-driven Alfven modes show frequency chirping down as mode moves out radially
- Simulations of fishbone instability show strong frequency chirping with large flattening region of particle distribution
- Plasma shaping (elongation) reduces α-particle stabilization significantly

Alpha Particle Stabilization of Internal Kink Mode for ITER:
Internal Kink Mode Structure

β_α=0.0

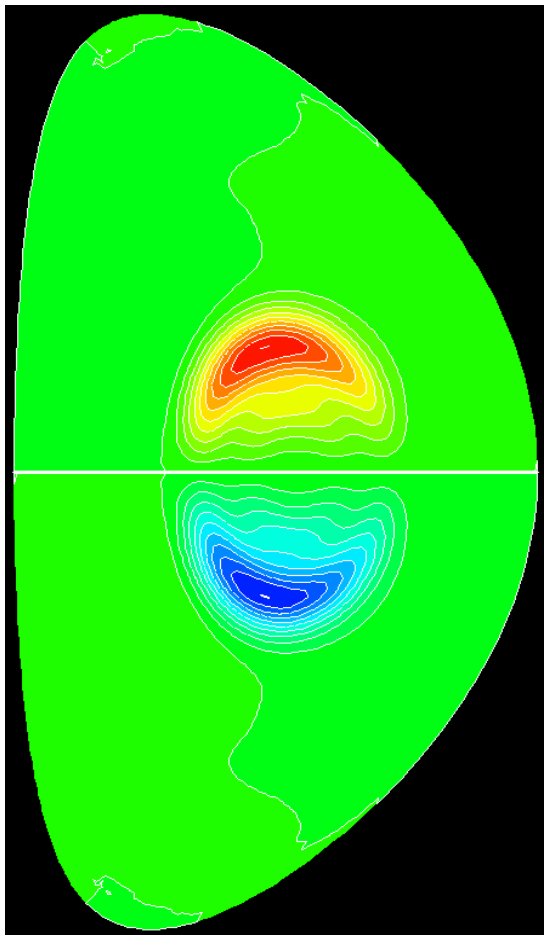

β_α=1.0%

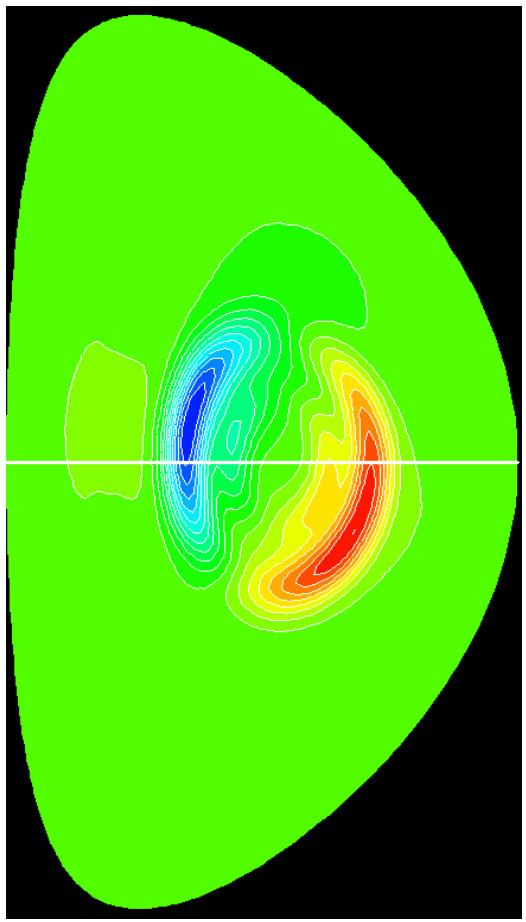

Fu

The stability of fishbone mode in ITER

Internal Kink / Fishbone studies have been extended to non-circular plasmas

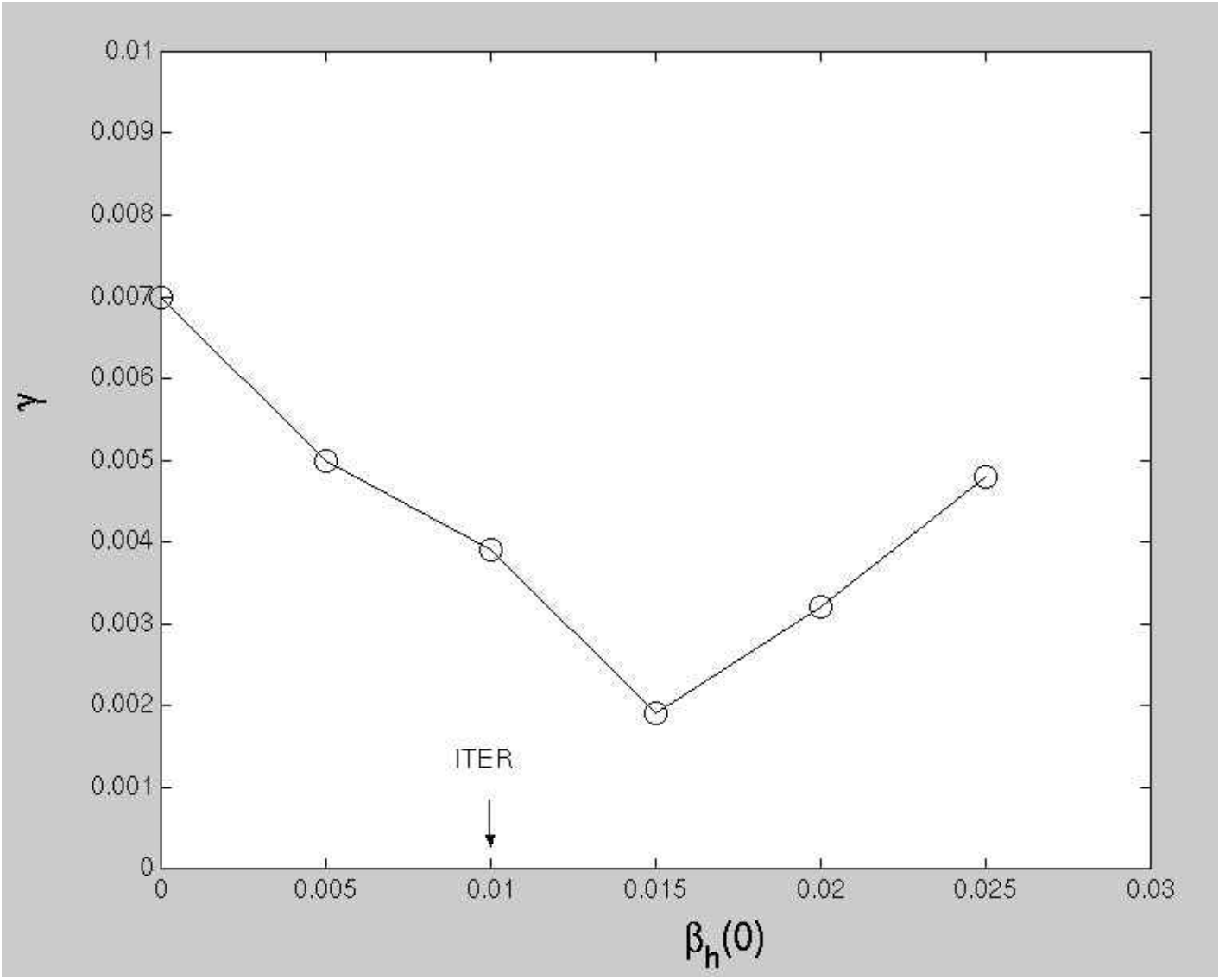

Fu

Thermal Ion Effects on Internal Kink Mode

Thermal ion kinetic effects reduce MHD growth rate of the internal kink by half (Kruskal-Oberman)

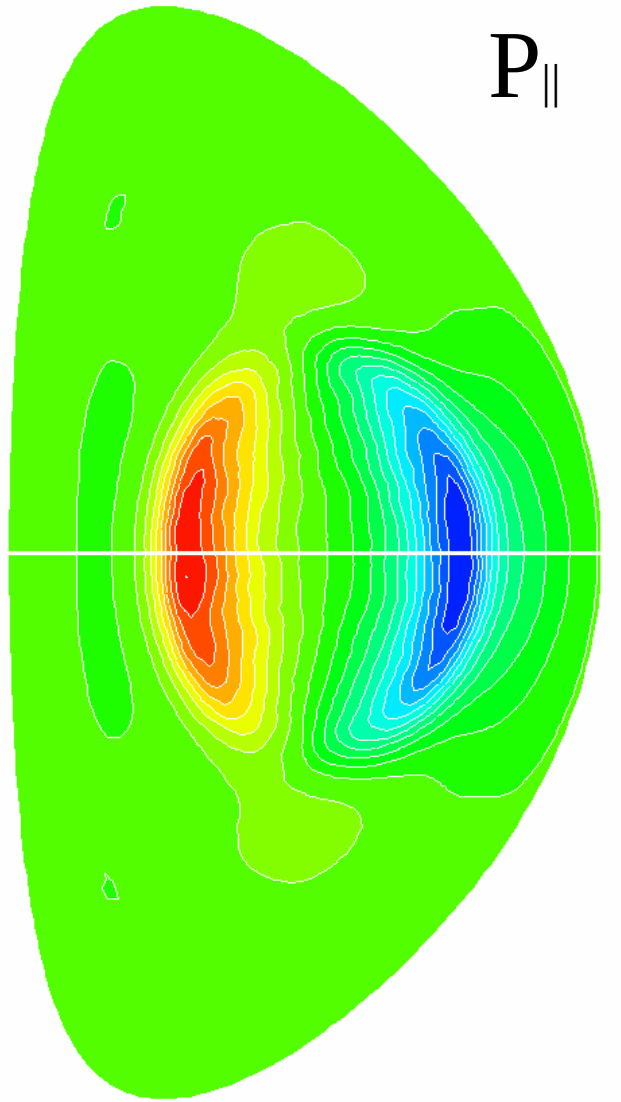

Fu

In nonlinear fishbone calculation, distribution function flattens and broadens and mode frequency chirps down.

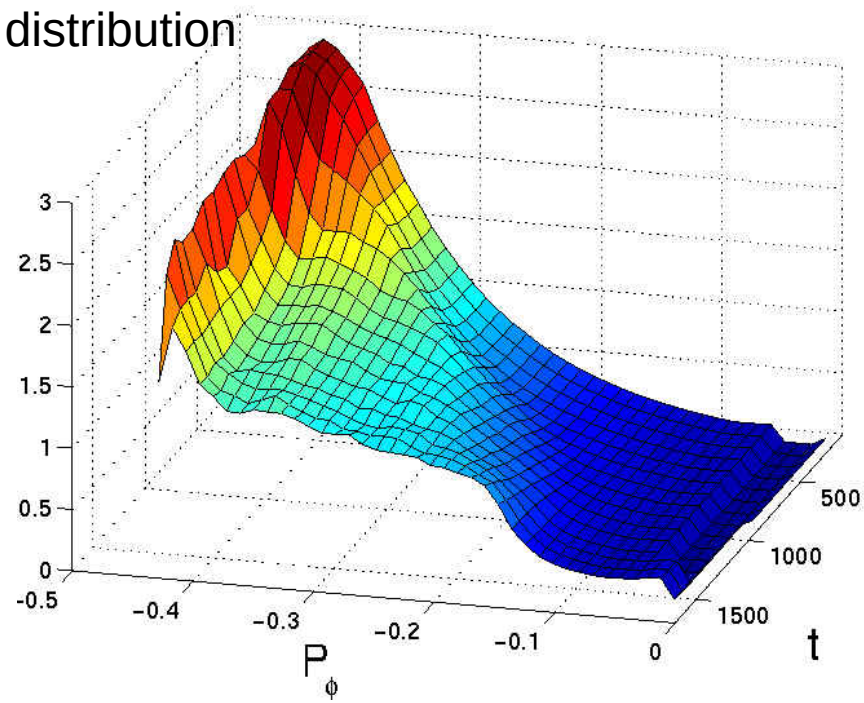

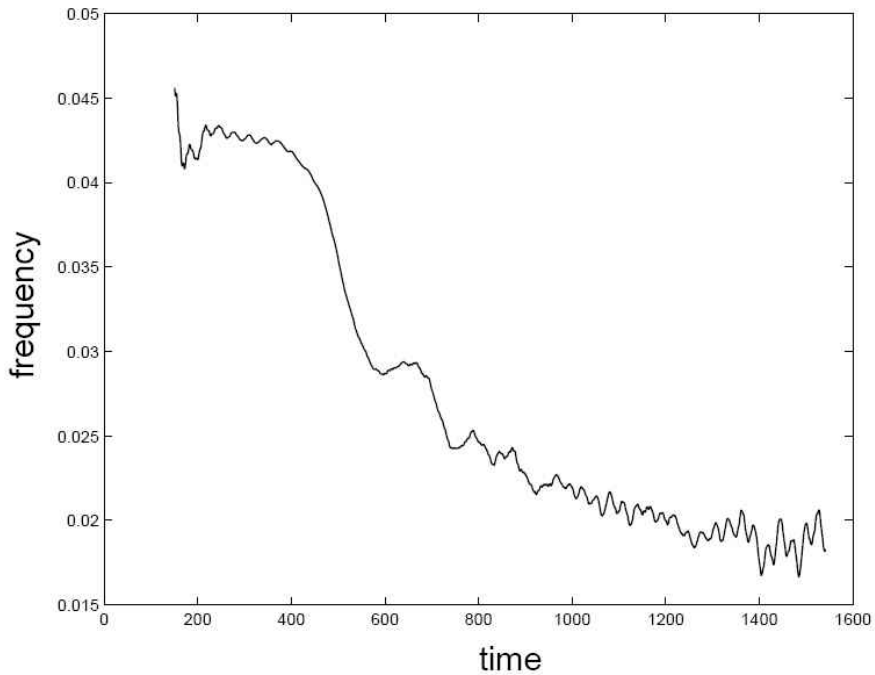

Fu

Physics Studies-4 (Pellet Injection)

- Combine global MHD simulations in a tokamak geometry with detailed local physics of pellet ablation
  - Includes ablation, ionization and electron heating in the neighborhood of the pellet
  - Competition between pellet material expanding along field line and localized instabilities causing cross field transport
- Goal is to develop predictive tool for design of fueling system for ITER
  - Velocity and size of pellet, launching angle
  - Tradeoffs between gas jet and pellet system
  - Use of pellets to induce smaller ELMs
  - Killer pellets for disruption mitigation

Progress in AMR Pellet Injection studies

- Introduced a non-orthogonal flux coordinate system into the CHOMBO AMR framework
- Implemented conservative finite volume upwind numerical method for MHD equations---now part of CHOMBO release
- Incorporated electron heat flux model by Ishizaki, Parks
- Demonstrated qualitative differences between inside and outside launch
- Implemented an implicit time advance in the uni-mesh code version that shows advantage for large mesh sizes
- Presented an invited talk at 2006 DPP-APS

Pellet Injection simulations

- Combine global MHD simulations in a tokamak geometry with detailed local physics including ablation, ionization and electron heating in the neighborhood of the pellet

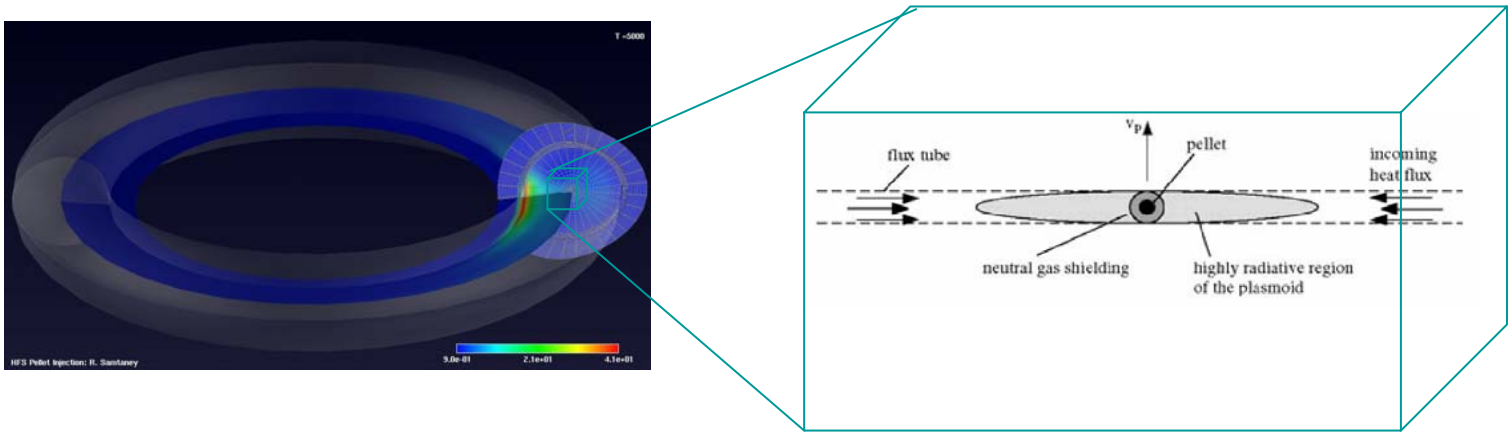

- AMR techniques to mitigate the complexity of the multiple spatial scales in the problem

Pellet Injection: AMR

- Meshes clustered around pellet
- Computational space mesh structure shown on right
- Mesh stats
  - 32^3 – base mesh with 5 levels, and refinement factor 2
  - Effective resolution: 1024^3
  - Total number of finite volume cells:113408
  - Finest mesh covers 0.015 % of the total volume
  - Time adaptivity: $1\ (\Delta t)_{base} = 32\ (\Delta t)_{finest}$

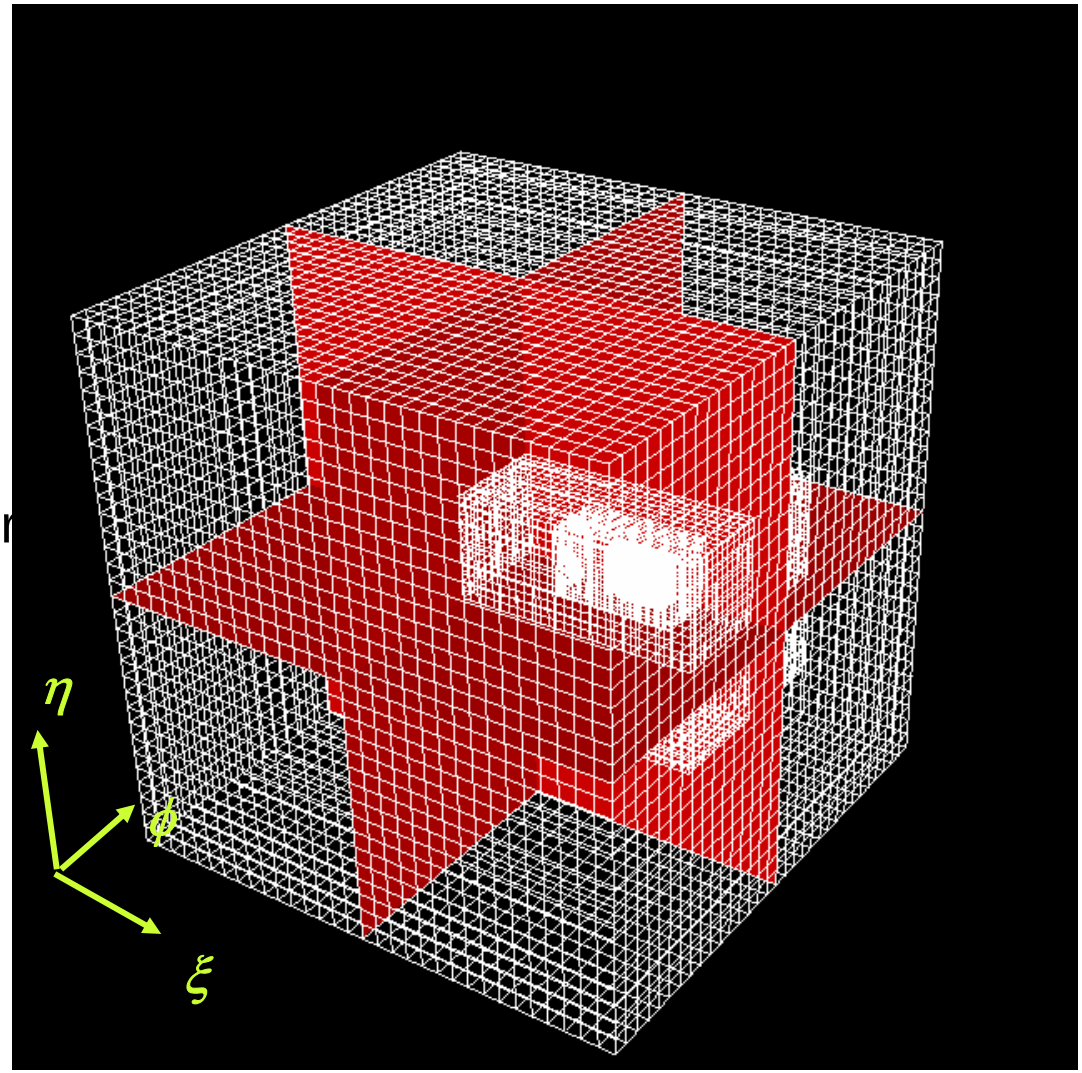

Samtaney

Pellet Injection: Pellet in Finest Mesh

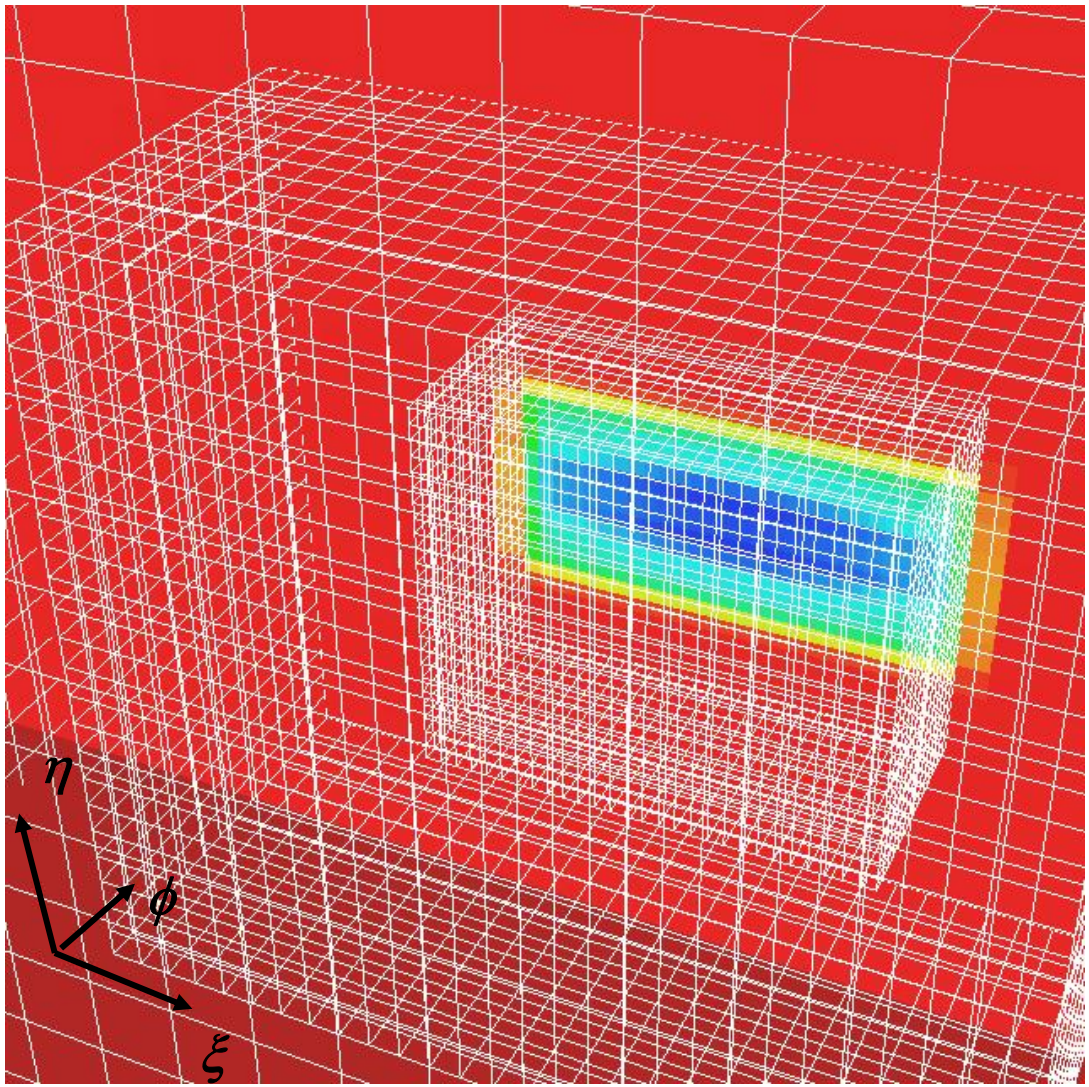

Samtaney

Results - HFS vs. LFS

B_T = 0.375T

$n_0=1.5\times10^{19}/m^3$

T_{e1}=1.3Kev

β=0.05

R_0=1m, a=0.3 m

Pellet: r_p=1mm,
v_p=1000m/s

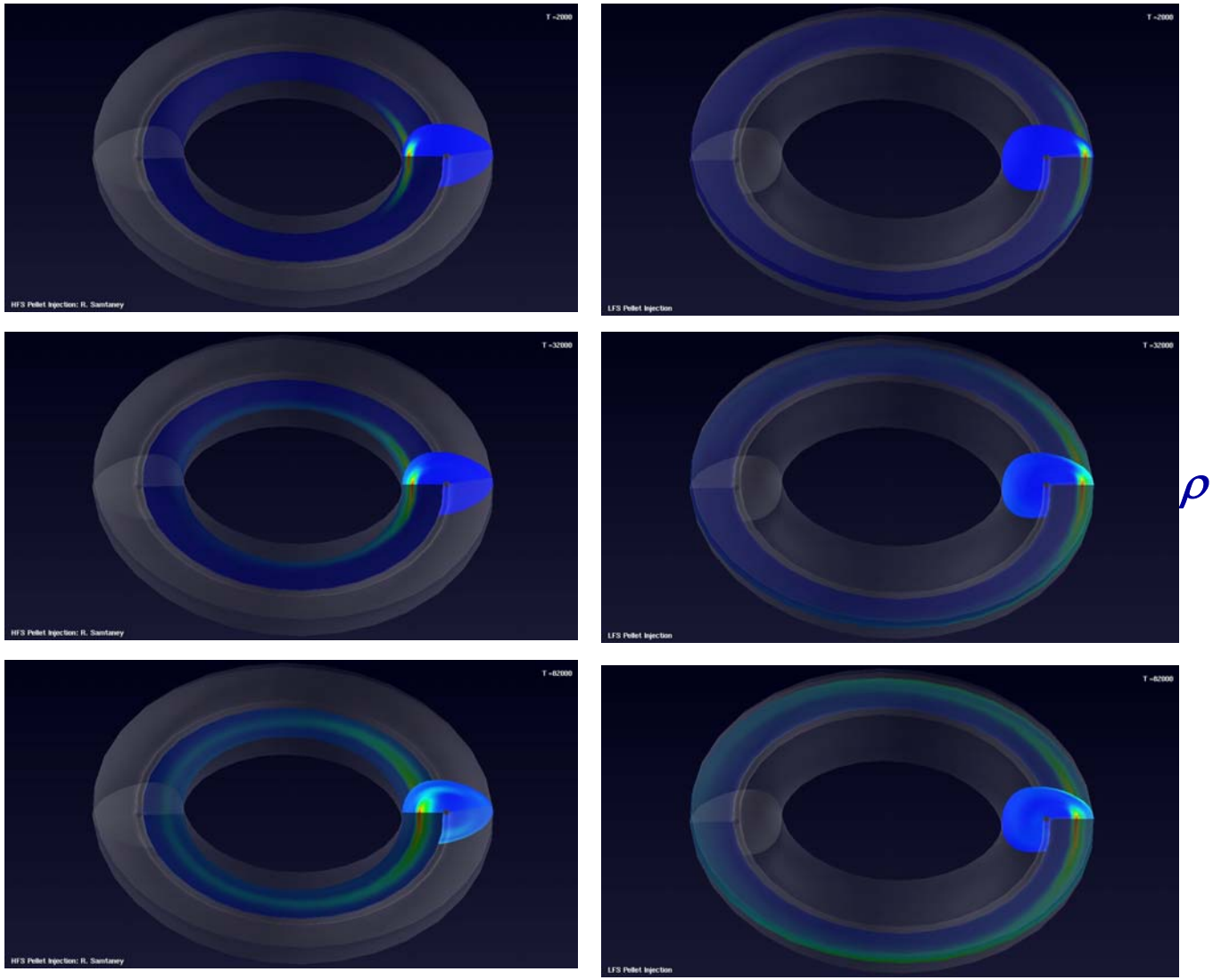

Samtaney

HFS vs. LFS - Average Density Profiles

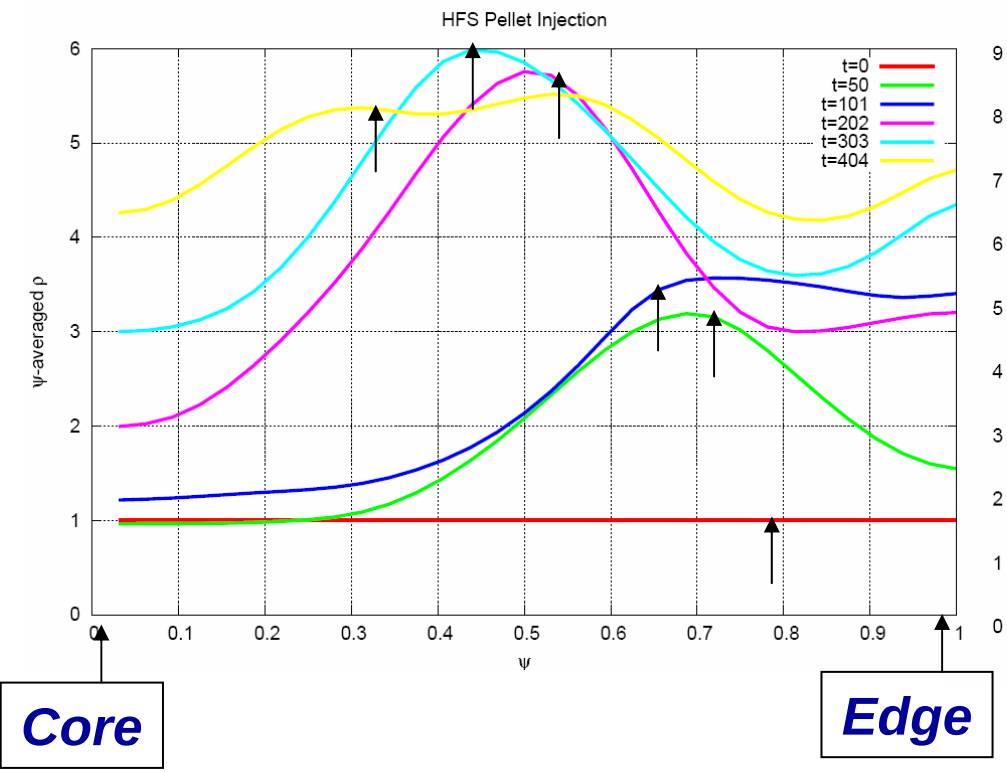

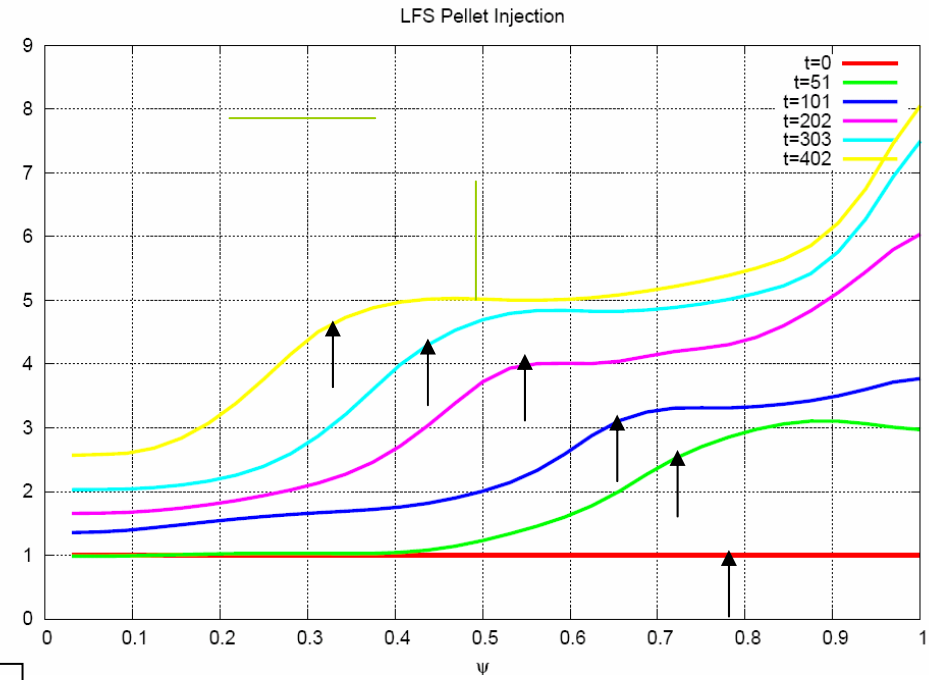

HFS Pellet injection shows better core fueling than LFS

Arrows indicate average pellet location

Samtaney

Pellet Injection - Exploring Jacobian Free Newton-Krylov Implicit Approach

- Choose a model problem with a similar separation of time scales (Reyolds et al. JCP 2006)

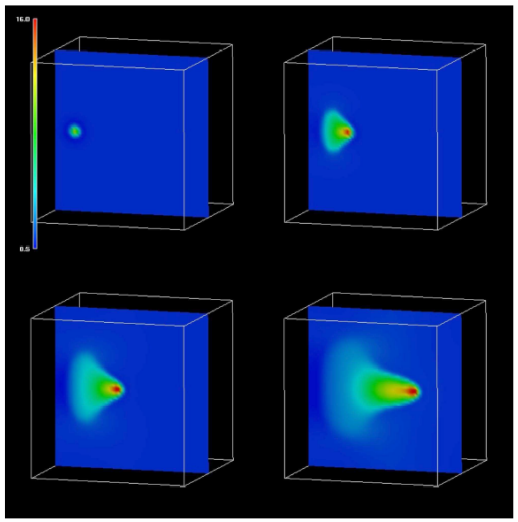

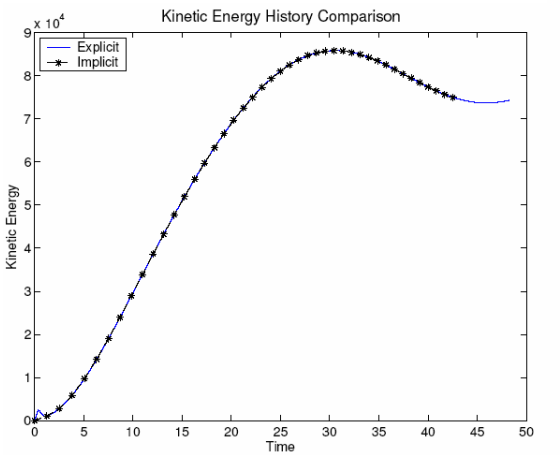

Good agreement between explicit and implicit methods

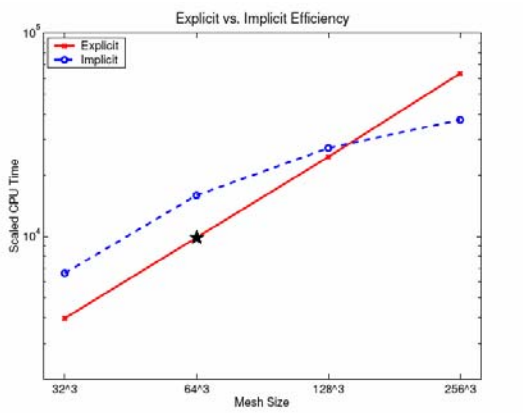

Implicit (no preconditioners) overtakes explicit method as problem size gets larger.

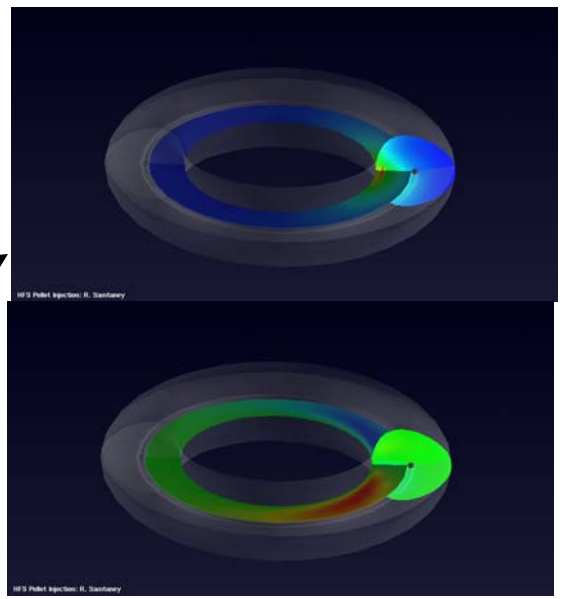

Implicit simulations in a toroidal geometry. $\Delta t = 100\ \Delta t_{explicit}$

Projecting to the Future

Scaling present CDX-U calculations to ITER parameters shows we need an additional 10^{12} space-time points (explicit, low order equivalent) to model ITER.

How to get an additional 12 orders of magnitude in 10-15 years?

- 1.5 orders: increased parallelism
- 1.5 orders: processor speed and efficiency
- 4 orders: adaptive gridding
- 1 order: higher order elements
- 1 order: field-line following coordinates
- 3 orders: implicit algorithms

Outline

- List of CEMM students and postdocs and their projects/thesis topics
- List of CEMM publications and invited conference presentations
- CEMM SciDAC Partners
- Description of the project meetings
- Closures progress and prospects
- Progress in numerical methods and numerical benchmarks
- Update on Major Physics Studies:
  - Sawtooth Simulations (CDX-U)
  - ELM Modelling (DIII-D)
  - Energetic Particle Modes (ITER)
  - Pellet Simulations
- Projecting to the future

BACKUP SLIDES

NIMROD Two-Fluid Algorithm

Development of a practical two-fluid algorithm that has no stability constraint on Δt and avoids numerical dissipation has been a critical task for NIMROD.

- After implementing and testing other approaches, we developed new **implicit leapfrog** algorithm that is based on the successful combination of NIMROD's semi-implicit resistive MHD advance and time-centered advection.
- The implicit Hall terms are linearized from the beginning of a step, resulting in second-order differential operators that are not self-adjoint.
- The resulting algebraic systems are smaller than with a centered implicit advance.
- Numerical analysis shows that the algorithm is unconditionally stable with flow, electron drift, Hall, and gyroviscous. effects.

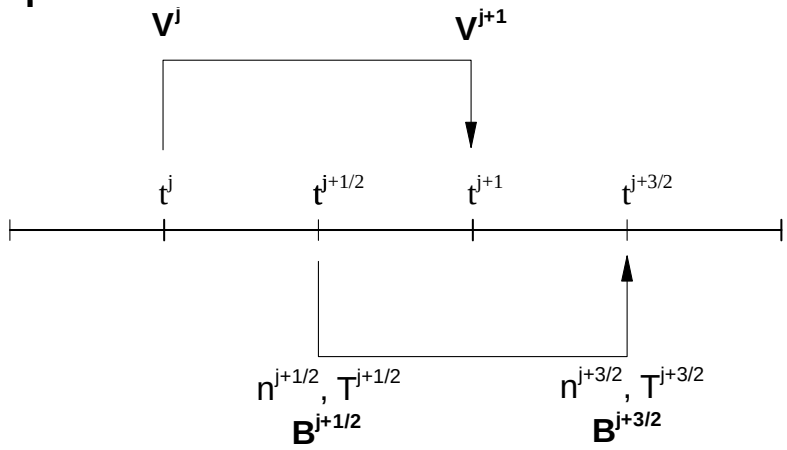

Schematic of temporal staggering.

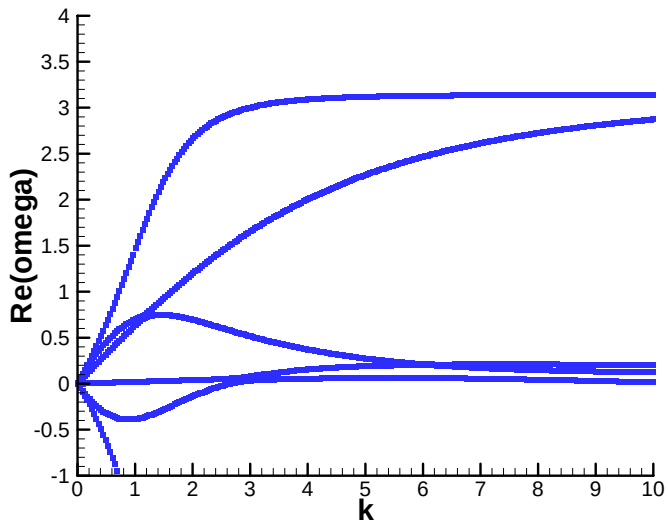

Sample numerical dispersion relation with flow and gyroviscosity.

NIMROD: Two-fluid Reconnection: Linear Tearing in Slab Geometry

- V. Mirnov, C. Hegna, and S. Prager apply asymptotics to sheared slab configurations over a wide range of parameters. [Phys. Pl. **11**, 4481 (2004)]
- The study extended and connected previous research on linear two-fluid tearing with a large guide field (B_z component).
- Using the new implicit leapfrog, we have run NIMROD on computations in conditions of large and small Δ' and large and small β.

	input					*output*		
CASE	$\Delta' L$	$k L$	β	ρ_s / L	$S \equiv \tau_r / \tau_a$	δ / L	$\Gamma \equiv \gamma \tau_a / k\rho_s$	Γ_{ana}*
A	0.28	0.93	0.002	0.56	6.7×10^{3}	0.184	8.51×10^{-3}	$\Gamma_{(54)}= 9.04\times10^{-3}$ $\Gamma_{(55)}=1.30\times10^{-2}$
B	0.28	0.93	0.083	3.6	6.7×10^{3}	0.172	1.50×10^{-3}	$\Gamma_{(56)}=1.61\times10^{-3}$
C	5.3	0.33	0.083	3.6	670	0.11	0.106	$\Gamma_{(73)}=0.109$
D	5.3	0.33	0.083	3.6	67	0.25	0.203	$\Gamma_{(73)}=0.221$
E	5.3	0.33	0.083	3.6	6.7	0.65	0.297	$\Gamma_{(73)}=0.379$
F	24	0.083	0.083	3.6	6.7	1.11	0.401	$\Gamma_{(68)}=0.550$
G	5.3	0.33	0.83	11.4	6.7	0.48	0.169	$\Gamma_{(73)}= 0.0928$

Comparison of computed growth rates (Γ) with analytical relations (Γ_{ana}) show good agreement when the reconnection layer (δ) is smaller than the equilibrium scale (L).